Author/s:
Delbridge, ARD;Kueh, AJ;Ke, F;Zamudio, NM;El-Saafin, F;Jansz, N;Wang, GY;Iminitoff, M;Beck, T;Haupt, S;Hu, Y;May, RE;Whitehead, L;Tai, L;Chiang, W;Herold, MJ;Haupt, Y;Smyth, GK;Thomas, T;Blewitt, ME;Strasser, A;Voss, AK

Title:
Loss of p53 Causes Stochastic Aberrant X-Chromosome Inactivation and Female-Specific Neural Tube Defects

Date:
2019

Citation:
Delbridge, A. R. D., Kueh, A. J., Ke, F., Zamudio, N. M., El-Saafin, F., Jansz, N., Wang, G. Y., Iminitoff, M., Beck, T., Haupt, S., Hu, Y., May, R. E., Whitehead, L., Tai, L., Chiang, W., Herold, M. J., Haupt, Y., Smyth, G. K., Thomas, T. ,... Voss, A. K. (2019). Loss of p53 Causes Stochastic Aberrant X-Chromosome Inactivation and Female-Specific Neural Tube Defects. Cell reports, 27 (2), pp.442-454.e5. https://doi.org/10.1016/j.celrep.2019.03.048.

Persistent Link:
https://hdl.handle.net/11343/370403

Article

Cell Reports

Loss of *p53* Causes Stochastic Aberrant X-Chromosome Inactivation and Female-Specific Neural Tube Defects

Graphical Abstract

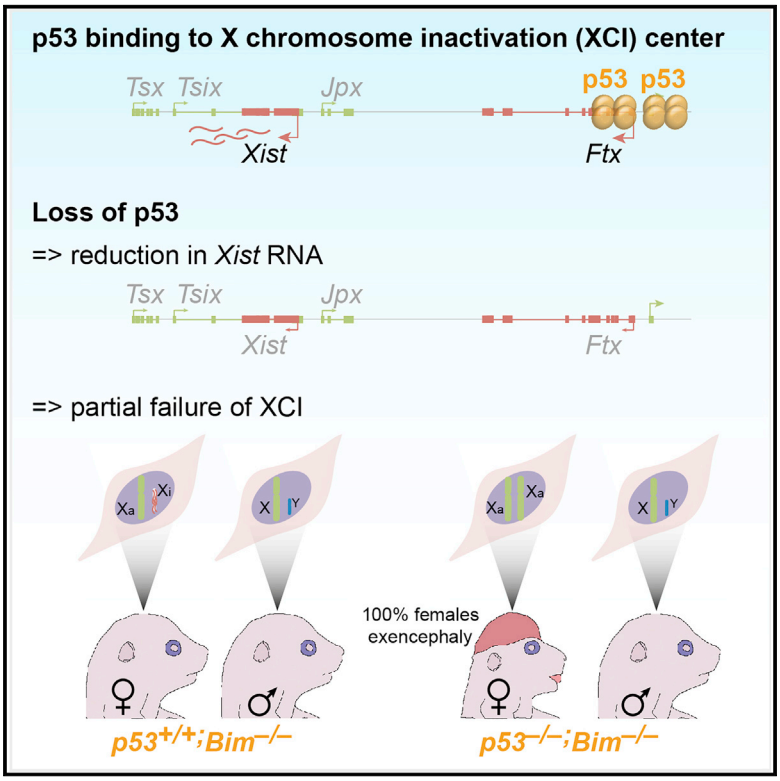

Highlights

- *p53/Bim* double knockout causes fully penetrant, female-specific neural tube defects
- p53 binds to sites in the X chromosome inactivation center
- Loss of p53 results in marked reduction of *Xist* RNA levels
- Absence of p53 causes biallelic expression of X chromosome genes

Authors

Alex R.D. Delbridge, Andrew J. Kueh, Francine Ke, ..., Marnie E. Blewitt, Andreas Strasser, Anne K. Voss

Correspondence

blewitt@wehi.edu.au (M.E.B.), strasser@wehi.edu.au (A.S.), avoss@wehi.edu.au (A.K.V.)

In Brief

The molecular mechanisms underlying the female bias of neural tube defects are currently unclear. Delbridge et al. present evidence that p53 is required for normal *Xist* expression and X chromosome inactivation and show in two models that partial failure of X chromosome inactivation is associated with female-biased neural tube defects.

Delbridge et al., 2019, Cell Reports *27*, 442–454
April 9, 2019
https://doi.org/10.1016/j.celrep.2019.03.048

CellPress

OPEN ACCESS
CellPress

Cell Reports
Article

Loss of *p53* Causes Stochastic Aberrant X-Chromosome Inactivation and Female-Specific Neural Tube Defects

Alex R.D. Delbridge,[1,2,8,9] Andrew J. Kueh,[1,2,9] Francine Ke,[1,2] Natasha M. Zamudio,[1] Farrah El-Saafin,[1,2] Natasha Jansz,[1,2] Gao-Yuan Wang,[1,3] Megan Iminitoff,[1] Tamara Beck,[1] Sue Haupt,[4,5] Yifang Hu,[1] Rose E. May,[1] Lachlan Whitehead,[1,2] Lin Tai,[1] William Chiang,[1,2] Marco J. Herold,[1,2] Ygal Haupt,[4,6] Gordon K. Smyth,[1,7] Tim Thomas,[1,2] Marnie E. Blewitt,[1,2,10,*] Andreas Strasser,[1,2,10,*] and Anne K. Voss[1,2,10,11,*]

[1]Walter and Eliza Hall Institute of Medical Research, Melbourne, VIC 3052, Australia
[2]Department of Medical Biology, The University of Melbourne, Melbourne, VIC, Australia
[3]College of Life Science, Zhejiang University, Hangzhou 310058, China
[4]Tumour Suppression Laboratory, Peter MacCallum Cancer Centre, Melbourne, VIC 3000, Australia
[5]Department of Clinical Pathology, The University of Melbourne, Parkville, VIC 3010, Australia
[6]Sir Peter MacCallum Department of Oncology, The University of Melbourne, Parkville, VIC, Australia
[7]School of Mathematics and Statistics, The University of Melbourne, Melbourne, VIC, Australia
[8]Present address: Multiple Sclerosis and Neuroimmunology Research Unit, Biogen, Cambridge, MA 02142, USA
[9]These authors contributed equally
[10]Senior authors
[11]Lead Contact
*Correspondence: blewitt@wehi.edu.au (M.E.B.), strasser@wehi.edu.au (A.S.), avoss@wehi.edu.au (A.K.V.)
https://doi.org/10.1016/j.celrep.2019.03.048

SUMMARY

Neural tube defects (NTDs) are common birth defects in humans and show an unexplained female bias. Female mice lacking the tumor suppressor p53 display NTDs with incomplete penetrance. We found that the combined loss of pro-apoptotic BIM and p53 caused 100% penetrant, female-exclusive NTDs, which allowed us to investigate the female-specific functions of p53. We report that female *p53*$^{-/-}$ embryonic neural tube samples show fewer cells with inactive X chromosome markers *Xist* and H3K27me3 and a concomitant increase in biallelic expression of the X-linked genes, *Huwe1* and *Usp9x*. Decreased *Xist* and increased X-linked gene expression was confirmed by RNA sequencing. Moreover, we found that p53 directly bound response elements in the X chromosome inactivation center (XIC). Together, these findings suggest p53 directly activates XIC genes, without which there is stochastic failure in X chromosome inactivation, and that X chromosome inactivation failure may underlie the female bias in neural tube closure defects.

INTRODUCTION

Neural tube defects (NTDs), such as exencephaly and *spina bifida*, are among the most common developmental defects and are observed at a frequency of 1 per 1,000 established pregnancies worldwide (Mitchell, 2005). At the severe end of the spectrum, NTDs, such as anencephaly and craniorachischisis, are lethal *in utero* or perinatally. NTDs of lesser severity can be treated with surgical intervention followed by ongoing management of neurological deficits and other complications, but they are commonly associated with severe disability (Copp et al., 2013).

NTDs result from failed neural tube closure during embryogenesis. Successful neural tube closure requires a complex interplay of several cellular and morphological processes that are still incompletely understood. Neural tube closure entails changes in the neural plate, whereby its lateral sides bend first dorsally, then medially, then elongate, and finally fuse at the dorsal midline to form a tube (Greene and Copp, 2014). Pertinent to this study, apoptosis is required for neural tube closure, as loss of several inducers or mediators of apoptosis can cause NTDs, including loss of APAF-1, caspase-9 or combined loss of caspases-3 and -7, or combined loss of BAX, BAK, and BOK (Cecconi et al., 1998; Hakem et al., 1998; Ke et al., 2018; Kuida et al., 1998; Lakhani et al., 2006; Yamaguchi et al., 2011; Yoshida et al., 1998).

For unknown reasons, females are over-represented among NTD cases, with various theories postulated to explain this phenomenon. X chromosome inactivation (XCI) is a dosage-compensation process specific to females and so has long been a contender for the cause of the female bias in NTDs (Hall, 1986), albeit unproven. An early effector of XCI is the long non-coding RNA *Xist*, which is expressed from the inactive X chromosome elect and subsequently recruits a series of epigenetic regulators that bring about silencing, including the polycomb repressive complexes (PRCs). *Xist* binds HnrnpK, which in turn recruits PRC1, catalyzing an epigenetic mark that recruits PRC2 (Almeida et al., 2017; Pintacuda et al., 2017). The mark laid down by PRC2, histone H3 lysine 27 methylation (H3K27me3), is a marker of the inactive X. The complete loss of XCI leads to developmental arrest in early embryogenesis; mice lacking *Xist*

function arrest at the egg cylinder stage (Hoki et al., 2009). In contrast, incomplete loss of XCI causes later developmental arrest with NTDs. Mice with a hypomorphic mutation of *Xist* arrest in development at embryonic day 9 (E9.0) and have an open neural tube (Senner et al., 2011). This suggests that, unlike complete loss of XCI, which causes developmental arrest in the egg cylinder stage, impaired XCI may cause NTDs.

Loss of the tumor suppressor p53 is one of approximately ten genetic alterations known to cause NTDs with a female bias (Armstrong et al., 1995; Harris and Juriloff, 2010; Sah et al., 1995; Slatter et al., 2011). p53 is a DNA-binding transcription factor and has a well-established role in the DNA damage response pathway, where, depending on cellular context, it can induce cell cycle arrest to allow DNA repair, cellular senescence, or apoptosis (Bieging and Attardi, 2012). p53 induces apoptosis through direct DNA binding and transcriptional activation of the genes encoding the pro-apoptotic BH3-only BCL-2 family members, PUMA and NOXA (Oda et al., 2000; Villunger et al., 2003). NTDs caused by loss of p53 are remarkable for the strong skewing of the sex ratio among affected individuals; 17%–60% of the female $p53^{-/-}$ embryos and only 0%–1% of the male $p53^{-/-}$ embryos display NTDs in at least three independent mouse strains (Armstrong et al., 1995; Sah et al., 1995; Slatter et al., 2011). None of the otherwise well-studied, known roles of p53 in the DNA damage response and apoptosis would explain the sex bias of the $p53^{-/-}$ NTDs. It is noteworthy that the $p53^{-/-}$ female bias does not appear to rely on the female sex per se but rather on the presence of two X chromosomes. XX mice that carry the male-sex-determining gene *Sry* on an autosome are phenotypically male, but some display the $p53^{-/-}$ NTDs. Conversely, XY mice with the *Sry* gene removed are phenotypically female and do not display the $p53^{-/-}$ NTDs (Chen et al., 2008). This raises the question of which mechanism necessitated by the presence of two X chromosomes may be faulty in $p53^{-/-}$ mice and lends further support to the idea that XCI may be a relevant mechanism, at least in the case of the $p53^{-/-}$ NTDs.

Neural tube closure is completed at E9.5 in the mouse. Therefore, mechanisms causing the female bias in neural closure must be examined at or before this time. Although the female bias of NTD in $p53^{-/-}$ was recognized over 20 years ago (Armstrong et al., 1995; Sah et al., 1995), the molecular mechanism by which loss of p53 causes female-specific NTDs has remained elusive, presumably in part due to the incomplete and variable penetrance, which hinders prospective investigation.

While investigating the impact of combined loss of p53 and the pro-apoptotic BH3-only BCL-2 family member BIM (Delbridge et al., 2016), we noticed serendipitously that the $p53^{-/-}$ female embryonic lethality and NTDs reached 100% penetrance. This provided us with the unique opportunity to prospectively isolate and examine female $p53^{-/-}$ embryos destined to develop NTDs and so allowed us to assess the role of p53 prior to the development of major anomalies in $p53^{-/-}$ embryos. We show here that loss of p53 causes defects in X chromosome inactivation in neural tissues and that p53 is required for normal levels of *Xist* RNA and directly binds response elements in the X chromosome inactivation center.

RESULTS

The loss of *p53* causes female-restricted NTDs with incomplete penetrance (loss of 17% to >60% of females, depending on strain and study; Armstrong et al., 1995; Sah et al., 1995), allowing examination of epistatic effects of additional mutations in genes encoding regulators of apoptosis. Specifically, we tested whether loss of the pro-apoptotic proteins BIM or BMF could increase the penetrance of NTDs or whether loss of the X-linked anti-apoptotic XIAP could reduce the penetrance of NTDs in $p53^{-/-}$ mice. The $p53^{-/-}$ males, which do not show NTDs (Armstrong et al., 1995; Sah et al., 1995), provided a control for gender-independent effects on neural tube closure. Diverse parental genotype combinations were used; therefore, the expected distributions of *p53*, *Bim*, *Bmf*, and *Xiap* offspring genotypes varied (Table S1). However, the expected female-to-male ratio remained 1:1 in all cases (Figure 1A), and this is the comparison we have used.

p53-Deficient Female Mice Are Underrepresented at 6 Weeks of Age, as Previously Reported

$p53^{-/-}$ and $p53^{+/-}$ mice were bred to produce $p53^{-/-}$ and $p53^{+/-}$ offspring, and offspring were genotyped after weaning. The sex distribution examined at 6 weeks of age indicated that only 19.6% of $p53^{-/-}$ offspring were female, and thus females were significantly underrepresented compared to the $p53^{+/-}$ controls (123:505 cf. the expected 1:1 ratio; $p < 10^{-6}$; Figure 1A; Table S1).

Loss of BIM Causes 100% Lethality of Female $p53^{-/-}$ Mice but No Obvious Impact on Male Mice

If loss of the pro-apoptotic function of p53 contributed to the NTDs and lethality in the $p53^{-/-}$ females, one might expect that, by removing a (p53-independent) inducer of apoptosis, the resulting reduction in developmental apoptosis might also increase the penetrance of lethality in $p53^{-/-}$ females, without affecting $p53^{-/-}$ males. To test this hypothesis, we generated mice that lacked both p53 and BIM, a potent BH3-only protein that can inhibit all pro-survival BCL-2 family members (Czabotar et al., 2014; O'Connor et al., 1998) and is critical for apoptosis induced by growth factor deprivation and certain other cytotoxic stimuli (Bouillet et al., 1999; Puthalakath et al., 2007). Of note, loss of BIM (Bouillet et al., 1999) alone does not cause NTDs.

Remarkably, loss of just a single *Bim* allele greatly increased the incidence of lethality of $p53^{-/-}$ females. Only 3.3% of $p53^{-/-}$;$Bim^{+/-}$ female mice survived to 6 weeks of age compared to 24.3% of $p53^{-/-}$ females (Figure 1A; $p < 0.001$; Fisher's exact test). In the complete absence of BIM, none of the $p53^{-/-}$ female mice reached 6 weeks of age ($p = 0.03$; Fisher's exact test; 0% versus 24.3%). Male $p53^{-/-}$ mice with or without additional loss of one allele of *Bim* were not underrepresented compared to other genotypes (Table S1). Complete loss of *Bim* on a p53 wild-type background ($Bim^{-/-}$) caused sex-independent embryonic lethality with ~50% penetrance (Table S1), as reported previously (Bouillet et al., 1999).

Similarly, we tested whether loss of BMF, BIM's closest relative (Puthalakath et al., 2001), which also contributes to growth-factor-deprivation-induced apoptosis (Labi et al.,

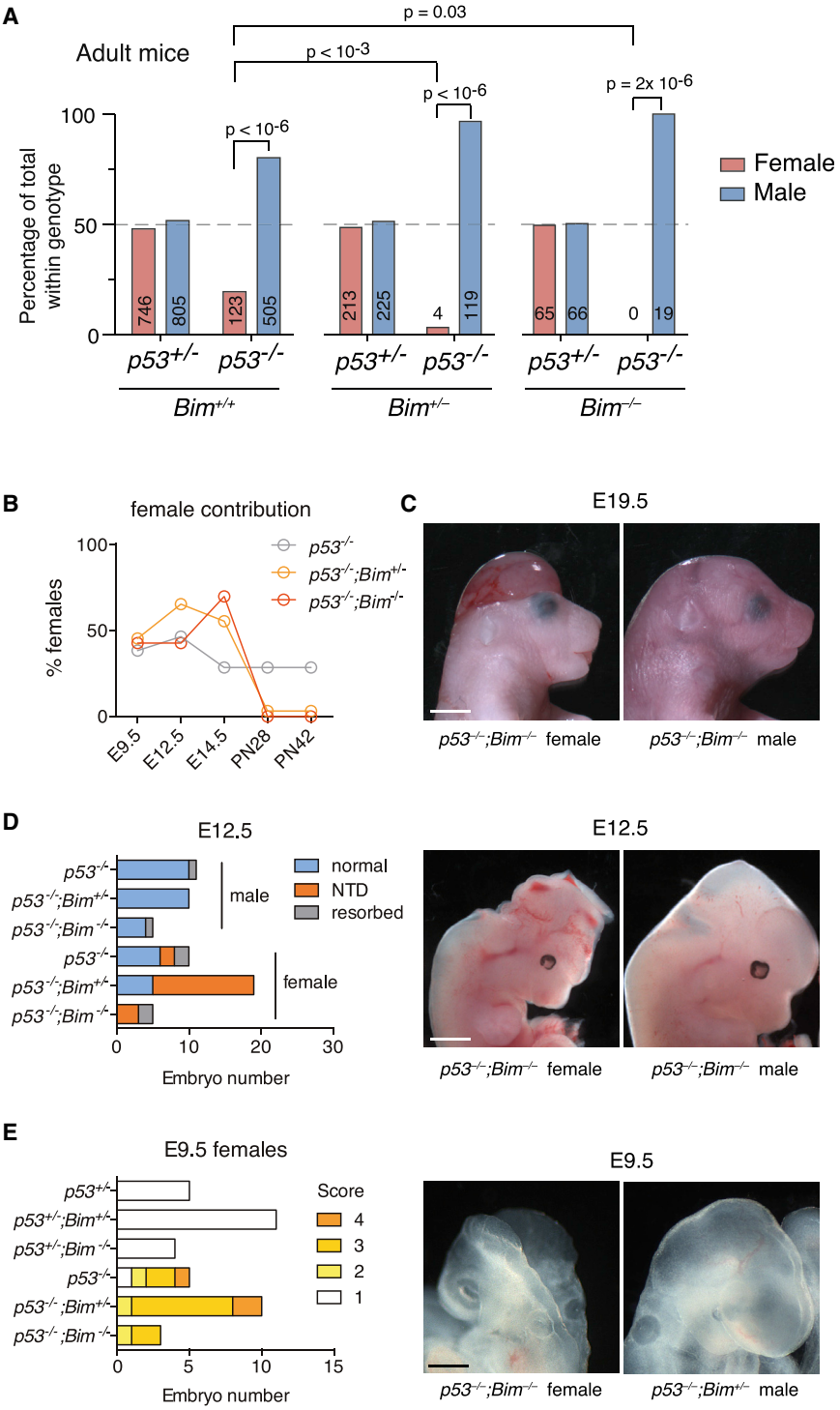

Figure 1. Loss of BIM Exacerbates the Developmental Lethality Observed in *p53*$^{-/-}$ Female Mice and Combined *p53*/*Bim* Deficiency Results in High-Penetrance Exencephaly

(A) *p53* mutant mice were crossed to mice deficient for the pro-apoptotic BH3-only BCL2 family member BIM. The numbers and percentages of male and female mice of the indicated genotypes were determined at 6 weeks of age. N, the number of animals is indicated in the bars. For sex distribution within a mouse strain, the cumulative binomial probability is presented. For comparison between strains, i.e., compound mutant data compared to *p53*$^{-/-}$ single mutant data (large brackets), Fischer's exact test was performed. Details on parental genotypes and all offspring genotypes are presented in Table S1. Related data on *p53*-deficient mice crossed to *Xiap*- or *Bmf*-deficient mice are displayed in Figure S1.

(B) Contribution of females of the indicated genotypes at various developmental time points. The number of animals per genotype examined was 7–58 (E9.5–E14.5) and 19–123 (postnatal day 28 [P28]–P42).

(C) Representative images of E19.5 pups.

(D) Incidence of NTDs in E12.5 embryos of the indicated genotypes with representative images. The number of animals per genotype examined is displayed in the bar graph.

(E) Extent of neural tube closure at E9.5 in female embryos of the indicated genotypes. "1" denotes normal closure, and "4" denotes complete failure of anterior neural tube closure. Representative images are shown. The number of animals per genotype examined is displayed in the bar graph.

Further data on the female *p53*$^{-/-}$ NTDs and staging by somite counts are displayed in Figure S1. The effects of loss of p53 and/or BIM on developmental apoptosis are displayed in Figure S2. Scale bars equal 3 mm (C), 710 μm (D), and 200 μm (E).

2008), affected the survival of female *p53*$^{-/-}$ mice. Loss of BMF (Labi et al., 2008) alone does not cause NTDs. Like *p53*$^{-/-}$ females, *p53*$^{-/-}$;*Bmf*$^{-/-}$ females were significantly underrepresented compared to males of the same genotype (5.5%; p = 0.00004; Figure S1A). The combined loss of BMF and p53 tended to further reduce the survival of females to 6 weeks of age, but this did not reach statistical significance (Figure S1A; p = 0.1; Fisher's exact test; 5.5% versus 24.3%).

Loss of the X-Linked Inhibitor of Apoptosis Did Not Affect the Underrepresentation of p53-Deficient Female Mice at 6 Weeks of Age

If loss of the pro-apoptotic function of p53 contributed to the NTDs and lethality in *p53*$^{-/-}$ females, one might expect that another regulator of apoptosis located on the X chromosome might contribute to the sex-biased death observed in the *p53*$^{-/-}$ females. The X-linked inhibitor of apoptosis (XIAP) is a critical inhibitor of apoptosis in certain contexts (Jost et al., 2009). Although the human *XIAP* gene is normally subject to X chromosome inactivation, *XIAP* is expressed at low levels (3% of the level of the active X) from the inactive

X and escaped from X chromosome inactivation in 7% of 43 lymphoblastoid and fibroblast cell lines (Cotton et al., 2013). Thus, based on its ability to inhibit apoptosis, the requirement for apoptosis in neural tube closure and its chromosomal localization, we tested XIAP as a possible contributor to the sex-biased nature of this phenotype. Like $p53^{-/-}$ females, $Xiap^{-/-};p53^{-/-}$ females were underrepresented (10 $Xiap^{-/-};p53^{-/-}$ females versus 48 males; $p < 10^{-6}$). However, loss of *Xiap* did not change the extent of female $p53^{-/-}$ underrepresentation at 6 weeks of age (Figure S1A; p = 0.6; Fisher's exact test; 20.8% versus 24.3%).

Female Embryos Lacking *p53* and One or Both Alleles of *Bim* Develop Neural Tube Defects with Complete Penetrance

We examined $p53^{-/-};Bim^{+/+}$, $p53^{-/-};Bim^{+/-}$, and $p53^{-/-};Bim^{-/-}$ embryos and compared them to control embryos at E9.5, E12.5, E14.5, and birth. Embryos were examined and scored blinded to genotype. As previously published (Armstrong et al., 1995; Sah et al., 1995), we observed female-specific NTDs associated strictly with the $p53^{-/-}$ genotype. Apart from the NTDs, we observed developmental delay in 2.4% of the embryos, which was not associated with any particular genotype. Developmentally delayed embryos (based on somite counts) were not used for further analysis (Figure S1). No other anomalies were observed. The proportions of females observed at E9.5, E12.5, and E14.5 were near 50%. However, between E14.5 and weaning, almost all $p53^{-/-};Bim^{+/-}$ as well as all $p53^{-/-};Bim^{-/-}$ female embryos were lost and the $p53^{-/-}$ female embryos (wild-type for *Bim*) were reduced to ~30% (Figure 1B). This indicates that the combined loss of p53 and BIM caused 100% lethality of the female fetuses in the last third of gestation or perinatally. The loss of 40% of $p53^{-/-}$ (wild-type for *Bim*) females also occurred during this period.

To gain further insight into the cause of the lethality of $p53^{-/-}$ females with compound loss of BIM, phenotypic analysis was performed at E19.5. In contrast to later time points, $p53^{-/-};Bim^{+/-}$ and $p53^{-/-};Bim^{-/-}$ female pups were readily observed and all presented with exencephaly (Figure 1C), which is incompatible with postnatal survival. To examine the early manifestations of the NTDs, embryos were analyzed at E9.5 and E12.5. At E12.5, all $p53^{-/-};Bim^{-/-}$ female embryos and the majority of $p53^{-/-};Bim^{+/-}$ female embryos exhibited prominent neural tube defects, primarily exencephaly (Figure 1D), and *spina bifida* was observed in a substantial number (Figure S1B). No NTDs were observed in male embryos of any genotype or any of the females that were not p53 deficient.

At E9.5, $p53^{-/-}$ females that also lacked either one or both alleles of *Bim* displayed obvious NTDs (Figure 1E). Embryos were scored blinded to genotype to quantitate the extent of neural tube closure on a scale from 1 to 4, with "1" equating to normal and "4" equating to embryos with severe failure of anterior neural tube closure (Figure S1C). This analysis revealed no overt differences in the spectrum of defect severity between $p53^{-/-};Bim^{-/-}$ and $p53^{-/-};Bim^{+/+}$ female embryos (Figure 1E). From this, we conclude that loss of BIM increases the penetrance of the NTDs in female mice lacking p53 but does not augment the severity or the nature of the defects observed.

Loss of *p53* or *Bim* Leads to a Reduction in Developmental Apoptosis but with No Difference between Sexes

Apoptosis in $p53^{-/-}$ female embryos and fetuses has been examined by histological methods (Armstrong et al., 1995) and TdT end labeling (TUNEL) on sections (Sah et al., 1995) and was reported to be indistinguishable from control embryos. In order to obtain spatial distribution data on apoptosis, we performed whole-mount (WM)-TUNEL on entire embryos. Corroborating previous histological reports (Armstrong et al., 1995; Sah et al., 1995), we did not detect differences in the distribution of TUNEL+ cells between $p53^{-/-};Bim^{+/-}$ and $p53^{+/+};Bim^{+/-}$ female or $p53^{-/-};Bim^{+/-}$ male E9.5 embryos (Figure S2A).

Fluorescence-activated cell sorting (FACS)-TUNEL has the potential to be more quantitative and more sensitive to changes than histological methods. FACS-TUNEL results revealed a lower proportion of TUNEL+ cells in male and female $p53^{-/-};Bim^{-/-}$ embryos compared to wild-type embryos (0.13% versus 1.62%; p = 0.003; Figures S2B and S2C). This effect was composed of independent effects of loss of p53 and loss of BIM in reducing developmental apoptosis (p53: p = 0.009; BIM: p = 0.04) that acted additively ($R^2 = 0.96$; p = 0.004; Figures S2D and S2E). Our results confirm the conclusion from a previous study (Armstrong et al., 1995) that a proportion of developmental apoptosis is independent of p53. However, as already presaged (Sah et al., 1995), we can now confirm a subtle reduction in developmental apoptosis in the absence of p53, with a further reduction with the additional loss of BIM. Pertinent to the female-specific $p53^{-/-}$ NTDs, there was no trend toward a difference in cell death between males and females (p = 0.5; Figures S2F and S2G).

Taken together, these findings suggest that the female specificity of the NTDs is unlikely to be due to the apoptosis-inducing roles of p53 and BIM. The roles of p53 and BIM in inducing apoptosis may, however, cooperate to sensitize embryos for NTDs caused by another female-specific, p53-dependent mechanism.

Loss of *p53* Results in a Reduction in the Proportion of Nuclei with a Detectable Inactive X Chromosome

Previous work indicated that the $p53^{-/-}$ NTDs, rather than being female specific, depended on the presence of two X chromosomes, suggesting that X chromosome inactivation might be involved (Chen et al., 2008). We therefore examined directly whether female $p53^{-/-};Bim^{+/-}$ cells had a defect in X chromosome activation.

We conducted experiments to detect the inactive X chromosome in E9.5 embryonic brain cells on a $Bim^{+/-}$ background using *Xist* fluorescence *in situ* hybridization (FISH), as well as by anti-H3K27me3 immunofluorescence (IF) staining. We observed a reduction in the percentages of cells with an inactive X chromosome, marked by *Xist* RNA accumulation or H3K27me3 enrichment, in brain cells from female $p53^{-/-}$ embryos compared to those from $p53^{+/+}$ female embryos (Figure 2A: 57% versus 75% cells with *Xist* RNA foci; Figure 2B: 37% versus 61% cells with H3K27me3 foci; $p < 0.0005$ in both cases). These findings suggest that X chromosome inactivation does not occur normally in a subset of brain cells in female E9.5 $p53^{-/-}$ embryos.

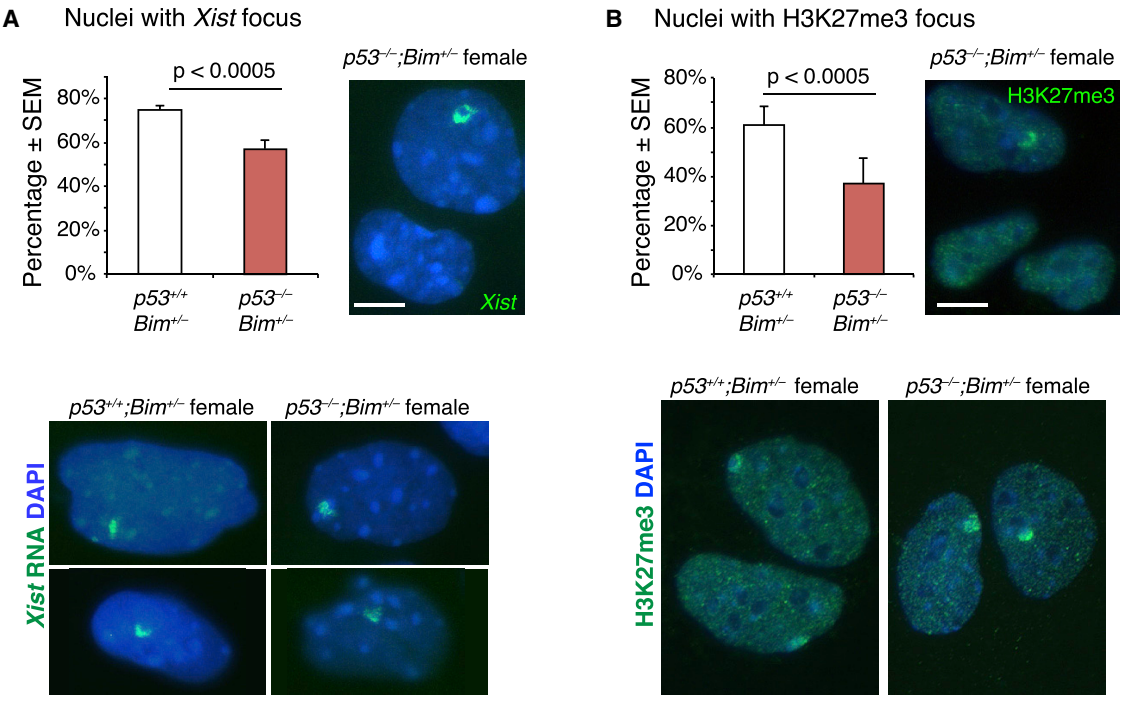

Figure 2. Loss of p53 Perturbs X Chromosome Inactivation in Female Embryos at E9.5

(A) Epifluorescence images of *Xist* RNA fluorescence *in situ* hybridization (FISH) marking the inactive X chromosome and assessment of the percentage of cells with a detectable *Xist*-positive focus in brain cells isolated from E9.5 $p53^{-/-};Bim^{+/-}$ and $p53^{+/+};Bim^{+/-}$ control brain cells.

(B) Anti-H3K27me3 immunofluorescence (IF) staining marking the inactive X chromosome and assessment of the percentages of cells with a detectable H3K27me3-positive focus.

Data in (A) and (B) are presented as mean ± SEM and were analyzed by Student's t test. An average of ~100 nuclei from 4 animals per genotype was examined for *Xist* clouds and from 5 animals per genotype for H3K27me3. Scale bars equal 8 μm, 9 μm, and 7 μm in (A) top, middle, and bottom, respectively and 8 μm in (B).

Loss of p53 Results in Biallelic Expression of X Chromosome Genes

The above described findings raised the question whether the cells without a *Xist* cloud or H3K27me3 focus found in the female p53-deficient embryos represented a failure of X inactivation. We therefore tested whether X chromosome genes were biallelically expressed in cells from female $p53^{-/-};Bim^{+/-}$ E9.5 embryos. We examined the expression of two X-linked genes subject to X inactivation, *Huwe1* and *Usp9x*, by nascent RNA FISH on brain cells of female E9.5 $p53^{-/-}$ ($Bim^{+/-}$ or $Bim^{+/+}$) embryos compared to control embryos ($p53^{+/+}$ or $p53^{+/-}$ with $Bim^{+/-}$ or $Bim^{+/+}$). We observed an increase in the percentage of cells with two *Huwe1* foci in female $p53^{-/-}$ cells compared to control cells (10% versus 3%, respectively; p = 0.04; Figures 3A and 3B). Biallelic expression was decisively more prominent in female $p53^{-/-}$ cells that also lacked a *Xist* cloud compared to cells with a *Xist* cloud (48% versus 3%, respectively; p = 0.025; Figure 3C). This suggests that the absence of *Xist* may contribute to the biallelic expression of *Huwe1*. Similarly, there was an increase in the percentage of cells with two *Usp9x* foci in female $p53^{-/-}$ cells compared to control cells (Figure 3D) and an increase in cells with biallelic expression of both *Huwe1* and *Usp9x* (12% versus 4%, respectively; Figure 3E). *Bim* status ($Bim^{+/-}$ or $Bim^{+/+}$) had no effect on the mono- or biallelic expression of *Huwe1* in p53-deficient female cells (Figure S3), implicating only p53 in the regulation of X chromosome inactivation.

As a positive control, we examined nascent *Huwe1* RNA in cells lacking the gene encoding the structural maintenance of chromosomes flexible hinge domain containing 1 protein (SMCHD1). SMCHD1 is essential for X chromosome inactivation (Blewitt et al., 2008). As reported previously for mouse embryonic fibroblasts (Mould et al., 2013), we observed that 29% of E9.5 $Smchd1^{MD1/MD1}$ (*Smchd1*-null) brain cells had biallelic expression of *Huwe1* compared to 1% in the control cells (Figures S4A and S4B). The extent of the biallelic expression was higher in the cells lacking SMCHD1 (29%; Figure S4B) than in the cells lacking p53 (10%–12%; Figures 3B and 3E).

Collectively, these data support the hypothesis that loss of p53 results in a partial failure of X chromosome inactivation.

Loss of p53 Results in Upregulation of X Chromosome Gene Expression, whereas *Xist* RNA Levels Are Reduced

To examine the effect of p53 loss more broadly on X-linked gene expression, we performed RNA sequencing on brain tissue from E9.5 $p53^{-/-};Bim^{+/-}$ female embryos, using as controls $p53^{-/-};Bim^{+/-}$ male embryos and $p53^{+/+};Bim^{+/-}$ female embryos. Embryos were matched for the number of somites to exclude an impact of any developmental delay that might occur (Figure S1E). By comparing the gene expression profiles between these three groups (Figures 4A and S5), we could identify the abnormally up- or downregulated genes that are specific for the NTD phenotype by first determining genes that are

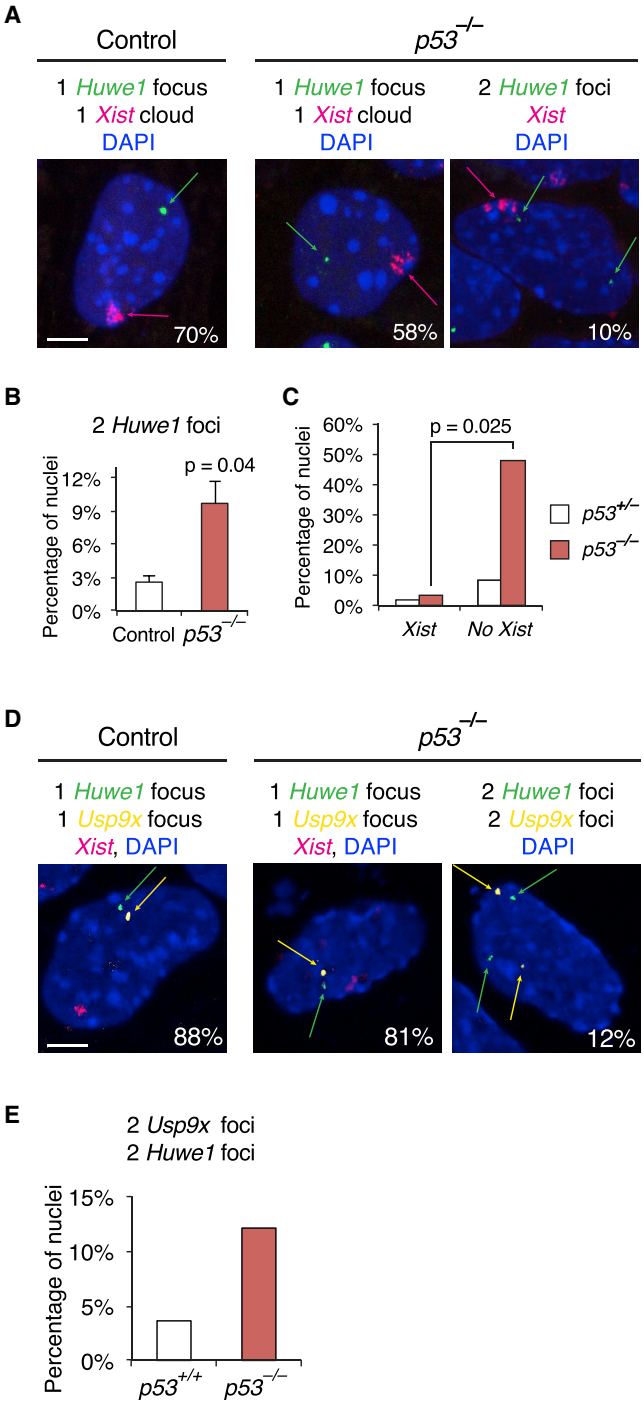

Figure 3. Loss of p53 Causes Biallelic Expression of Genes Ordinarily Subject to X Chromosome Inactivation

(A) Confocal images of nascent *Huwe1* RNA FISH and *Xist* RNA FISH in brain cells isolated from E9.5 $p53^{-/-}$ and control ($p53^{+/+}$ or $p53^{+/-}$) embryos.

(B) Numerical assessment of nuclei with biallelic expression of *Huwe1*.

(C) Percentage of nuclei with biallelic expression of *Huwe1* among cells with or without *Xist* cloud.

(D) Confocal images of nascent *Huwe1* and *Usp9x* RNA FISH in E9.5 brain cells.

(E) Numerical assessment of nuclei with biallelic expression of both *Huwe1* and *Usp9x*.

differentially expressed due to the absence of p53 ("affected females" [AFs] = $p53^{-/-};Bim^{+/-}$ females versus "control females" [CFs] = $p53^{+/+};Bim^{+/-}$) and second excluding those genes that are not associated with NTD ("control males" [CMs] = $p53^{-/-};Bim^{+/-}$ males unaffected by NTD versus control females = $p53^{+/+};Bim^{+/-}$). These genes are thus specific to animals that lack *p53* and exhibit a NTD (Figure 4A).

The top differentially expressed gene was *Ccng1* encoding cyclin G1, a well-established target gene of p53 (Okamoto and Beach, 1994). However, *Ccng1* mRNA levels were decreased in both male and female $p53^{-/-};Bim^{+/-}$ embryos compared to the $p53^{+/+};Bim^{+/-}$ female control embryos (Figure S5B), ruling it out as a candidate for the female-specific NTDs. The second top differentially expressed gene was the X chromosome inactivation gene *Xist*, which was downregulated in the female $p53^{-/-};Bim^{+/-}$ embryos compared to the $p53^{+/+};Bim^{+/-}$ female control embryos (Figure S5B). The top 12 differentially expressed genes included 3 genes located on the X chromosome and ordinarily subject to X chromosome inactivation, *Capn6*, *Irs4*, and *Maob*, which were upregulated in the female $p53^{-/-};Bim^{+/-}$ embryos compared to the $p53^{+/+};Bim^{+/-}$ female control embryos and control male $p53^{-/-};Bim^{+/-}$ embryos (Figure S5B). Downregulation of *Xist* and upregulation of genes ordinarily subject to X chromosome inactivation support the hypothesis of a defect in X chromosome inactivation in the female $p53^{-/-};Bim^{+/-}$ brain tissue.

Overall, we observed a 2.3-fold enrichment of X chromosome genes among the genes upregulated in $p53^{-/-};Bim^{+/-}$ females versus control $p53^{+/+};Bim^{+/-}$ females (Roast test p = 0.0006; Figures 4B, 4C, and S5B), although in contrast, genes that initiate X chromosome inactivation located within the X inactivation center (XIC) were downregulated (Roast test p = 0.0002; Figures 4B, 4C, and S5B), including *Xist* (Figures 4B and 4C; down 3-fold; false discovery rate [FDR] = 0.0002). Comparison of control $p53^{+/+};Bim^{+/-}$ females with control $p53^{-/-};Bim^{+/-}$ males showed efficient X chromosome dosage compensation with very few X chromosome genes differentially expressed with genome-wide significance (Figure 4D). In contrast, many X chromosome genes were upregulated in $p53^{-/-};Bim^{+/-}$ females compared to control $p53^{-/-};Bim^{+/-}$ males, indicating a defect in X chromosome dosage compensation (Figure 4D). Similarly, X chromosome genes were upregulated in $p53^{-/-};Bim^{+/-}$ females compared to control $p53^{+/+};Bim^{+/-}$ females (Figure 5A). The decrease in *Xist* RNA levels and the increase in mRNA levels of genes ordinarily subject to dosage compensation in $p53^{-/-};Bim^{+/-}$ females compared to control $p53^{+/+};Bim^{+/-}$ females and control $p53^{-/-};Bim^{+/-}$ males were corroborated by qRT-PCR using independent samples of E9.5 brain tissue

Data in (B) are presented as mean ± SEM and were analyzed by Student's t test (B) or Pearson Chi^2 test (C). 599 control nuclei ($p53^{+/+}$ or $p53^{+/-}$) from 3 animals and 1,116 $p53^{-/-}$ nuclei from 5 animals were assessed for *Huwe1*. 374 $p53^{+/-}$ nuclei and 460 $p53^{-/-}$ nuclei from two animals each for *Huwe1*/*Xist* are shown. 225 $p53^{+/+}$ nuclei from one animal and 656 $p53^{-/-}$ nuclei from 3 animals for *Huwe1*/*Usp9x* are shown. Related data are displayed in Figure S3, and results for a protein known to be essential for XCI, SMCHD1, are shown in Figure S4 as a positive control. Scale bars equal 4 μm, 5 μm, and 5 μm in (A) left to right and 4 μm, 5 μm, and 5 μm in (B) left to right.

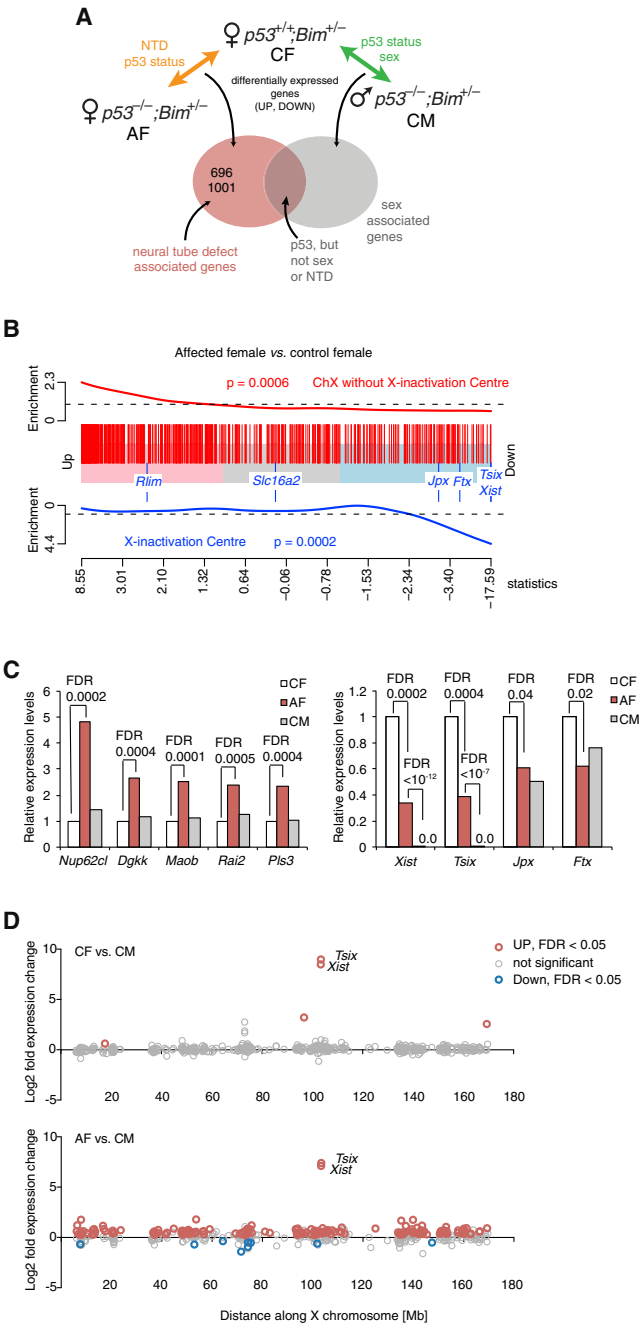

Figure 4. Loss of p53 Leads to Deregulation of Gene Expression from the X Chromosome in Female Embryos at E9.5

(A) Analysis strategy, including differentially expressed genes depicting comparison groups: $p53^{-/-};Bim^{+/-}$ (AFs, neural tube defect [NTD] affected females); $p53^{+/+};Bim^{+/-}$ (CFs, control females); and $p53^{-/-};Bim^{+/-}$ (CMs, control males). 3 to 4 animals per genotype were used in the RNA sequencing experiment.

(B) Barcode plot depicting significant enrichment of X chromosome genes within the upregulated genes (by moderated t-statistic) in the AF versus CF comparison (red; Roast test; p = 0.0006), although X genes located in the X chromosome inactivation center are downregulated (blue and labeled; Roast test; p = 0.0002).

(C) Relative expression levels of examples of upregulated X chromosome genes and of genes encoding non-coding RNAs involved in X chromosome inactivation.

(D) Chromosome view of the $\log_2$-fold change in X chromosome gene expression depicting dosage compensation of the two X chromosomes in CF compared to CM and the failed X chromosome dosage compensation in AF compared to CM.

Data in (C) are presented as relative mean reads per kilobase of transcript, per million mapped reads (RPKM). All data were analyzed as detailed in the STAR Methods under RNA sequencing. All differentially expressed genes are displayed in Table S2. Further RNA sequencing data are presented in Figure S5.

(Figures 5B and 5C). The overall expression from the X chromosome differed from all other chromosomes. It was the only chromosome that showed an overall upregulation (Roast test FDR 0.01) in female $p53^{-/-};Bim^{+/-}$ brain tissue compared to the $p53^{+/+};Bim^{+/-}$ control females (or $p53^{-/-};Bim^{+/-}$ males; not shown). Overall gene expression from all other chromosomes is either not significantly affected by the absence of p53 or reduced (Figure 5D).

In addition to X chromosome genes, many other genes were differentially expressed. However, these genes did not correlate significantly with NTDs in previous studies. Indeed, genes that, when mutated, cause NTDs were generally upregulated in the absence of p53 (Figures S5C and S5D).

These findings support the hypothesis that loss of p53 compromises X chromosome dosage compensation and is required for the normal levels of *Xist* RNA.

p53 Binds to Enhancers in the X Chromosome Inactivation Center

Prior to X chromosome inactivation, *Xist* expression is repressed (Kay et al., 1993), although *Tsix* is robustly expressed from the anti-parallel DNA strand (Lee et al., 1999). When *Jpx* expression is triggered, *Xist* expression is upregulated on the X chromosome that is destined to be inactivated (Tian et al., 2010), whereas, conversely, *Tsix* is downregulated. The *Xist* transcript spreads from the XIC to coat the X chromosome (Clemson et al., 1996). *Xist* expression sets off a cascade of changes, including enrichment in H3K27me3 (Plath et al., 2003; Silva et al., 2003). H3K27me3 is a repressive mark, laid down by the PRC2. These and other changes mediate chromatin condensation and repression of gene expression on the inactive X chromosome (for review, see Dixon-McDougall and Brown, 2016). The *Ftx* locus is located within the XIC and has been proposed to be important for *Xist* expression (Chureau et al., 2011; Furlan et al., 2018).

To explore the mechanism by which p53 might regulate genes involved in X chromosome inactivation, we analyzed the X inactivation center for putative p53 binding sites. We examined an anti-p53 chromatin immunoprecipitation (ChIP) sequencing dataset (Li et al., 2012) for sites of p53 binding and found two prominent binding sites near the *Ftx* locus (*Ftx_1* and *Ftx_2*; Figure S6A). These two sites were clearly occupied by p53 in untreated embryonic stem cells (ESCs) and had enhanced occupation in doxorubicin-treated ESCs (Figure S6A); doxorubicin-induced DNA damage causes activation and stabilization of p53. DNA sequence analysis revealed that the two sites contained p53 consensus binding sites. We isolated $p53^{+/+}$ and $p53^{-/-}$ ESCs from E3.5 embryos of $p53^{+/-}$ × $p53^{+/-}$ matings and cultured them with and without doxorubicin and subjected

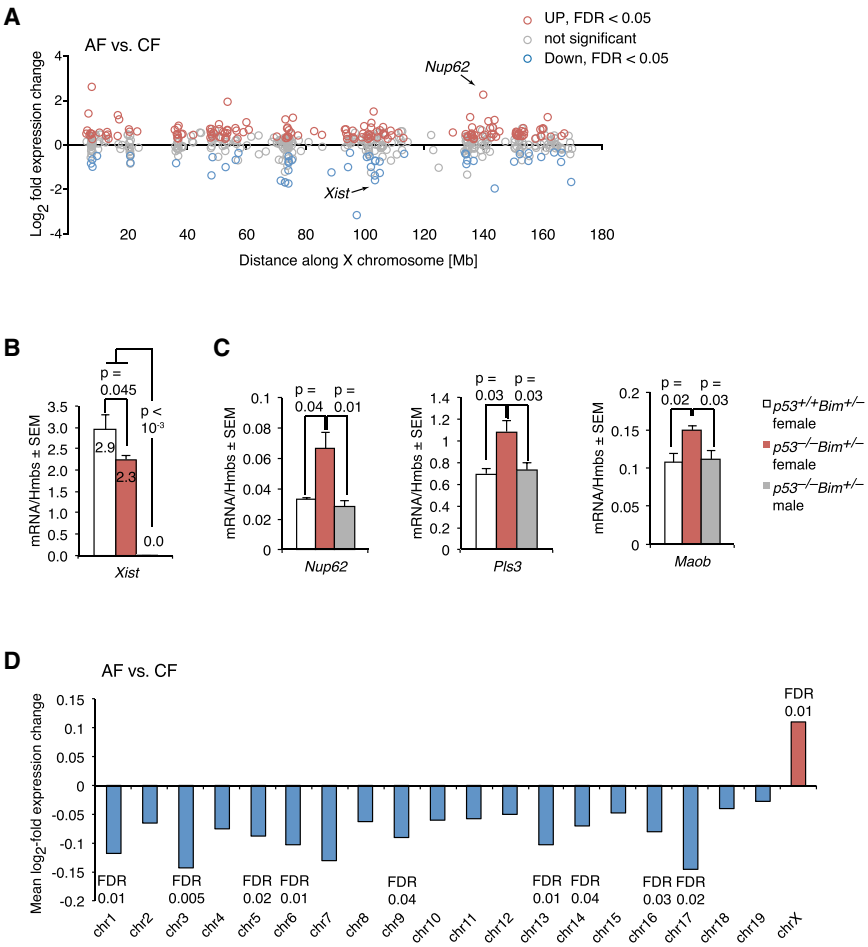

Figure 5. Confirmation of the Reduction in *Xist* RNA Levels and Increase in RNA Levels of Genes Ordinarily Subject to X Chromosome Inactivation

(A) Chromosome view of the $\log_2$-fold change in X chromosome gene expression between $p53^{-/-}$;$Bim^{+/-}$ (AFs) and $p53^{+/+}$;$Bim^{+/-}$ (CFs). Data were analyzed as detailed in the STAR Methods under RNA-sequencing.

(B and C) Confirmation of the (B) reduction in *Xist* RNA levels and (C) increase in RNA levels of genes ordinarily subject to X chromosome inactivation on samples of brain tissue from female $p53^{-/-}$;$Bim^{+/-}$, male $p53^{-/-}$;$Bim^{+/-}$, and female $p53^{+/+}$;$Bim^{+/-}$ E9.5 embryos by qRT-PCR. Samples were independent of those used for RNA sequencing. Data are shown as mean mRNA levels normalized to housekeeping genes ± SEM and were analyzed by one-way ANOVA followed by Bonferroni test. N = 3 or 4 animals per genotype.

(D) Assessment of overall gene expression changes between AF and CF per chromosome. Mean $\log_2$-fold changes in gene expression per chromosome are shown.

3 to 4 animals per genotype were used in the RNA sequencing experiment. Data were analyzed by Roast test, as detailed in the STAR Methods under RNA sequencing. p53 binding to sites in the XIC, as well as p53 reporter gene transactivation mediated by the p53 binding sites in the XIC, are displayed in Figure S6. Related data are displayed in Figures S7 and S8.

these cells to anti-p53 ChIP-qPCR. We observed p53 occupancy at the sites near the *Ftx* locus in untreated $p53^{+/+}$ ESCs and enhanced occupancy in doxorubicin-treated $p53^{+/+}$ ESCs and no signal in the $p53^{-/-}$ negative control ESCs (Figure S6B). To examine whether the p53 binding sites near the *Ftx* locus resulted in transactivation, we cloned both sequences individually into luciferase reporter constructs. Reporter assays in p53-deficient H1299 cells showed that enforced expression of p53 was sufficient to drive luciferase gene expression using either the *Ftx_1* or the *Ftx_2* p53 binding site, with *Ftx_2* conferring greater transactivation (Figure S6C).

The p53 binding site *Ftx_1* resides within the *Ftx* gene, and *Ftx_2* is located upstream of the *Ftx* gene. The sites contain transcription factor binding sites and active chromatin marks (CTCF, POL2, p300, cJUN, H3K4me1, and H3K4me3). This suggests that deletion of these sites would not just affect p53's ability to activate XIC genes but also interfere with the function of other transcription factors and the *Ftx* gene, which itself is required for *Xist* expression. Deletion of *Ftx* exons 1–5, which include p53 binding site *Ftx_1*, causes a 4-fold reduction in *Xist* RNA levels (Chureau et al., 2011), similar to loss of p53. We therefore did not pursue mutational analysis of these sites.

The p53 binding sites near the *Ftx* locus were the only pronounced p53 binding sites found in the XIC, but because they are distant from the transcriptional start site (TSS) of the *Xist* gene, we also used an established algorithm (ConSite; Sandelin et al., 2004) to detect putative sites closer to the *Xist* gene. We detected several high-ranking putative p53 binding sites proximal to the *Jpx* TSS and two putative binding sites proximal to *Xist*. However, none of these putative binding sites displayed p53 binding as assessed by anti-p53 ChIP-qPCR, and they were unable to mediate p53-dependent transactivation in luciferase reporter assays (Figure S7).

These data, representing a survey of confirmed and putative p53 binding sites of the X chromosome inactivation center, suggest that p53 directly binds to sites in the vicinity of the *Ftx* locus to promote transcriptional activation of one or more X chromosome inactivation genes.

As an alternative mechanism potentially conferring female-specific NTDs, it has been proposed that female cells are more susceptible to limiting levels of epigenetic repressors, because maintenance of X chromosome inactivation recruits a large proportion of the available chromatin repressors (Juriloff and Harris, 2012). To investigate this possibility, we examined p53 occupancy and expression of genes encoding chromatin modifiers. Although p53 binding was detected in the vicinity of some gene loci encoding chromatin repressive proteins, the effects of loss of p53 on these gene loci appeared to be relatively mild

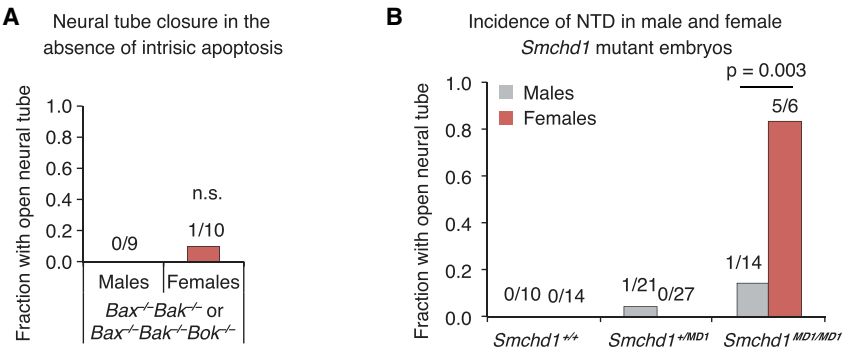

Figure 6. Impaired X Chromosome Inactivation, but Not Lack of Apoptosis, Is Associated with Female-Specific NTDs

(A) The incidence of NTDs in the absence of intrinsic apoptosis is low. $Bax^{-/-}Bak^{-/-}$ double-knockout and $Bax^{-/-}Bak^{-/-}Bok^{-/-}$ triple-knockout embryos are completely deficient for intrinsic apoptosis (Ke et al., 2018).

(B) Strong female bias of NTDs in embryos lacking SMCHD1. SMCHD1 is essential for X chromosome inactivation (Blewitt et al., 2008) and Figure S4.

The numbers of animals examined are indicated in the bar graphs. Fractions of the total numbers of embryos are displayed. Data were analyzed by Pearson's chi-squared test.

(Figure S8). This suggests that, in the case of the NTDs caused by loss of p53, this mechanism would only make a small contribution to the pronounced female specificity.

Defective X Chromosome Inactivation, but Not Obliteration of Developmental Apoptosis, Causes Female-Specific NTDs

Based on the observation that the reduction in apoptosis in $p53^{-/-}$ embryos (independent of *Bim* genotype) is not female-specific (Figure S2) and the observation that loss of p53 causes a reduction in *Xist* RNA levels and a defect in X chromosome dosage compensation, which is a female-specific process, we would propose that the effects of p53 on X chromosome gene expression underlie the female specificity of the NTDs in the $p53^{-/-}$ mice, not the effects of p53 on apoptosis. Nevertheless, the loss of developmental apoptosis in $p53^{-/-};Bim^{-/-}$ embryos clearly brought about a higher penetrance of the female-specific NTDs. Based on these findings, we hypothesized that, although loss of developmental apoptosis by means other than loss of p53 may cause NTDs, these would not be sex biased and, conversely, that defective X chromosome inactivation caused by means other than loss of p53 would cause female-specific NTDs. To test this hypothesis, we examined mouse embryos lacking the pro-apoptotic BCL-2 family effector proteins BAX, BAK, and BOK and mouse embryos lacking the X chromosome inactivation protein SMCHD1. We have shown previously that $Bax^{-/-}Bak^{-/-}$ double-knockout and $Bax^{-/-}Bak^{-/-}Bok^{-/-}$ triple-knockout embryos have no detectable developmental cell death (Ke et al., 2018) and that SMCHD1 is essential for X chromosome inactivation (Blewitt et al., 2008).

Consistent with our previous study (Ke et al., 2018), we observed low penetrance of NTDs in E11.5 $Bax^{-/-}Bak^{-/-}$ and $Bax^{-/-};Bak^{-/-};Bok^{-/-}$ embryos (Figure 6A), suggesting that loss of developmental apoptosis by itself was not a candidate mechanism for the 100% penetrance of the NTDs in the $p53^{-/-};Bim^{-/-}$ mice, although the decrease in apoptosis observed in both male and female $p53^{-/-};Bim^{-/-}$ may predispose to NTDs. In contrast, among embryos lacking SMCHD1 and thus having defects in X chromosome inactivation (Blewitt et al., 2008; Figure S4), 5 of 6 female $Smchd1^{MD1/MD1}$ embryos, but only 1 of 14 male $Smchd1^{MD1/MD1}$ embryos, had NTDs (Figure 6B).

These data indicate that defects in X chromosome inactivation caused by loss of two unrelated proteins (SMCHD1 or p53) can lead to female-specific NTDs with high penetrance.

DISCUSSION

The data presented here identify female-specific molecular and cellular changes associated with the female-specific neural tube defects in *p53*-deficient mice. In the absence of p53, we observed (1) the absence of *Xist* clouds and H3K27me3 foci in a subset of cells, (2) biallelic expression of X chromosome genes, (3) increased expression of genes ordinarily subject to X chromosome inactivation, and (4) reduced expression of the X chromosome inactivation center genes, most notably *Xist*, *Jpx*, and *Ftx*. We demonstrated (5) p53 binding to specific sites in the X chromosome inactivation center and (6) its ability to activate reporter gene transcription based on binding to these sites. Lastly, we used two unrelated methods of reducing developmental apoptosis and impairing X chromosome inactivation to show that (7) impaired X chromosome inactivation, but not lack of developmental apoptosis alone, can cause female-specific, highly penetrant NTDs.

A number of studies provided evidence that loss or reduction in apoptosis from the peri-implantation stage onward causes NTDs (Cecconi et al., 1998; Hakem et al., 1998; Ke et al., 2018; Kuida et al., 1998; Lakhani et al., 2006; Yoshida et al., 1998), and one study presented evidence that apoptosis is not required for the specific time period of neural tube closure (Massa et al., 2009). Together, the studies suggest that accumulation of cells throughout development due to lack of apoptosis in a range of tissues, including the neural tube, can cause NTDs, even if apoptosis may not be acutely required during the process of neural tube closure. Thus, we propose that loss of p53-induced apoptosis predisposes to NTDs. A reduction in apoptosis occurred in both male and female $p53^{-/-}$ embryos, and we suggest that, combined with a defect in XCI, this causes failure of neural tube closure specifically in the female embryos. The additional loss of pro-apoptotic BIM further raises the threshold for apoptosis initiation, thus accounting for the enhanced penetrance of the NTDs in $p53^{-/-};Bim^{+/-}$ and $p53^{-/-};Bim^{-/-}$ females.

It has long been postulated that the preponderance of females affected by NTDs is derived from defective X chromosome

inactivation (Hall, 1986). However, this hypothesis had not been readily accepted, in part because complete failure of X chromosome inactivation results in very early lethality. For example, female carriers of paternally inherited loss-of-function allele of *Xist* die at E6.5 (Hoki et al., 2009). Of note, loss of p53 (or SMCHD1) does not cause complete failure of XCI at E9.5 (with ~88% and 71% of cells still displaying monoallelic expression, respectively). We therefore hypothesize that the failure of XCI in only a subset of cells is compatible with development beyond E6.5 and that neural tube closure is a developmental process, during which partial failure of XCI causes noticeable problems. In agreement with this hypothesis, mice carrying a hypomorphic allele of *Xist* display NTDs (Senner et al., 2011). Further congruent with our proposal, NTDs in $p53^{-/-}$ mice have been attributed to the presence of two X chromosomes rather than the absence of a Y chromosome or the physical sex (Chen et al., 2008).

Apart from direct binding within the XIC and transactivation of XIC genes, p53 could also potentially affect *Xist* expression indirectly in the following manner. The pluripotency factor Nanog has been shown to repress the *Xist* gene (Navarro et al., 2008), and p53 has been reported to repress the *Nanog* gene (Lin et al., 2005) in mouse embryonic stem cells. Collectively, these studies would suggest that loss of p53 could result in an increase in *Nanog* mRNA and protein, which could result in a more pronounced repression of *Xist.* It is possible that such indirect mechanisms operate in addition to a direct regulation of XIC genes by p53. Furthermore, p53 may activate *Xist* indirectly through activation of the *Ftx* locus, as deletion of *Ftx* resulted in a significant reduction in *Xist* expression (Chureau et al., 2011; Furlan et al., 2018).

The absence of *Xist* and H3K27me3, as well as biallelic expression of X chromosome genes, was observed in p53-deficient female embryos at the time of neural tube closure on embryonic day 9.5, which is unusual, as cells that fail XCI ordinarily are considered not to persist. This suggests that the level of XCI failure in the $p53^{-/-}$ female cells at ~12% may not be severe enough to trigger elimination. It is worth noting, however, that the fate of cells failing to undergo XCI during development is not known. These cells may remain in the population, may be actively selected against, or disassemble their *Xist* cloud(s) and re-enter cell division (Monkhorst et al., 2008). Based on our investigation of the role of apoptosis in development (Ke et al., 2018), the cells failing to undergo XCI are unlikely to die by apoptosis, because we did not see sex-biased effects of the combined loss of BAX, BAK, and BOK, the critical effectors of apoptosis.

Our observations at E9.5 cannot distinguish whether XCI failed at initiation, establishment, or during maintenance. In this context, it is worth noting the *Xist* RNA is not required for the maintenance of XCI in mouse embryonic fibroblasts (Csankovszki et al., 1999). Nevertheless, we have shown that p53 binds to sites within the XIC at the *Ftx* locus and others suggested that the *Ftx* locus may act as an enhancer of *Xist* (Furlan et al., 2018). Therefore, we propose that p53 may be required for the efficient activation of genes within the XIC, such as *Xist* and/or *Ftx*, and that the absence of p53 may compromise initiation of XCI. In this context, it is noteworthy that the 5′ end of the *Ftx* locus, the region where we observed p53 binding, has been shown to engage in long-range interactions with the *Xist* locus (Furlan et al., 2018). These may bring p53 bound to the sites at the 5′ end of the *Ftx* locus into physical contact with the transcriptional machinery at the *Xist* locus, an interaction that would enable *Xist* transactivation by p53. Mutational analysis of the p53 binding sites detected in the XIC may be useful to determine whether their mutation causes female-specific NTDs.

p53 is a well-known transcription factor with a range of functions (Bieging and Attardi, 2012), so it was surprising to find that only 18 genes were differentially expressed between the $p53^{-/-}$ males and $p53^{+/+}$ control females, compared to 3,718 genes differentially expressed between $p53^{-/-}$ female and $p53^{+/+}$ control female brains. The latter are likely to include effects that are secondary to defects in brain development. The female-specific NTDs may be caused by the mis-regulation of a large number of genes rather than a small number of specific regulators of neurogenesis. Noteworthy in this context is that the average directional gene expression changes from individual chromosomes were either unchanged or downregulated, except for the X chromosome, which stood out with an average upregulation.

Apart from loss of p53, mutations in several other genes have been reported to result in female-biased NTDs (reviewed in Juriloff and Harris, 2012). However, the expression of these genes was not noticeably affected by the absence of p53 in our study (even with the additional loss of BIM), and thus, the mechanisms underlying the female specificity of their loss-of-function phenotype remain to be determined.

In conclusion, we have shown that the 17%–60% penetrance of NTDs in $p53^{-/-}$ female mice rises to 100% when the pro-apoptotic protein BIM is also lost. Our finding supports the notion that the $p53^{-/-}$ NTDs are mediated by a sex-independent component, i.e., loss of the pro-apoptotic function of p53, combined with a sex-specific component, i.e., a defect in X chromosome inactivation. Importantly, we observed biallelic and increased gene expression from the X chromosome but a loss of gene expression in the XIC, including *Xist* gene expression, and a loss of formation of repressed X chromosome chromatin in a subset of the $p53^{-/-}$ female embryonic brain cells. Our data suggest that this results from a defect in the activation of *Xist* gene expression by p53, independent of p53's function in apoptosis. How cells with biallelic expression of X chromosome genes affect neural tube closure at the level of tissue morphogenesis remains to be determined.

STAR★METHODS

Detailed methods are provided in the online version of this paper and include the following:

- KEY RESOURCES TABLE
- CONTACT FOR REAGENT AND RESOURCE SHARING
- EXPERIMENTAL MODEL AND SUBJECT DETAILS
  - Mice
  - Isolation of p53 mutant and control ES cells
- METHOD DETAILS
  - Phenotypic analysis
  - Whole-mount TUNEL staining and microscopy
  - TUNEL staining for flow cytometric analysis

SUPPLEMENTAL INFORMATION

Supplemental Information can be found online at https://doi.org/10.1016/j.celrep.2019.03.048.

ACKNOWLEDGMENTS

We thank Drs. C. Scott, T. Jacks, A. Villunger, T. Kaufmann, D.C.S. Huang, S.J. Korsmeyer, C. Thompson, J.M. Adams, and P. Bouillet for gifts of mice; Moshe Oren, Antonio Constanzo, and Giovanni Blandino for provision of reagents; K. Humphries, K. Walker, E. Lanera, J. Mansheim, G. Siciliano, S. O'Connor, K. Trueman, G. Dabrowski, and K. Vella for expert animal care; and B. Helbert, H. Ierino, K. Mackwell, and C. Young for mouse genotyping. C. Scott was responsible for the initial mating of the $Bim^{-/-}$ and $p53^{-/-}$ strains and generously bequeathed this colony. This work was supported by grants and fellowships from the Cancer Council of Victoria (A.R.D.D., Sydney Parker Smith Postdoctoral Research Fellowship), the National Health and Medical Research Council (program grant no. 1016701; SPRF Fellowship 1020363 to A.S.; SRF Fellowships 575512 and 1081421 to A.K.V.; PRF Fellowship 1058892 and program grant 1054618 to G.K.S.; project grants 1051078 and 1084504), the Leukemia and Lymphoma Society (SCOR grant no. 7001-13), the estate of Anthony (Toni) Redstone OAM, Australian Postgraduate Awards (A.R.D.D., N.J., and F.E.-S.), The Bellberry-Viertel Senior Medical Research Fellowship (M.E.B.) and Cancer Therapeutics CRC Top-up Scholarship (A.R.D.D.), the Peter MacCallum Cancer Foundation (S.H.) and NHMRC 1123057, and National Breast Cancer Foundation IN-16-042 (Y. Haupt). This work was made possible by operational infrastructure grants through the Australian Government IRISS and the Victorian State Government OIS.

AUTHOR CONTRIBUTIONS

The study was conceived by A.R.D.D. and A.S. Experiments were designed by A.S., A.K.V., A.J.K., and A.R.D.D., with contributions from N.J., S.H., Y. Haupt, F.E.-S., G.K.S., M.J.H., and M.E.B. Experiments were conducted and analyzed by A.R.D.D., A.J.K., F.K., N.M.Z., F.E.-S., N.J., G.-Y.W., M.I., T.B., S.H., Y. Hu, R.E.M., L.W., L.T., W.C., M.J.H., T.T., G.K.S., and A.K.V. The manuscript was prepared by A.R.D.D., A.J.K., A.S., and A.K.V. with help from the other authors.

DECLARATION OF INTERESTS

The authors declare no competing interests.

Received: February 20, 2018
Revised: February 11, 2019
Accepted: March 13, 2019
Published: April 9, 2019

REFERENCES

Almeida, M., Pintacuda, G., Masui, O., Koseki, Y., Gdula, M., Cerase, A., Brown, D., Mould, A., Innocent, C., Nakayama, M., et al. (2017). PCGF3/5-PRC1 initiates polycomb recruitment in X chromosome inactivation. Science *356*, 1081–1084.

Armstrong, J.F., Kaufman, M.H., Harrison, D.J., and Clarke, A.R. (1995). High-frequency developmental abnormalities in p53-deficient mice. Curr. Biol. *5*, 931–936.

Bieging, K.T., and Attardi, L.D. (2012). Deconstructing p53 transcriptional networks in tumor suppression. Trends Cell Biol. *22*, 97–106.

Blewitt, M.E., Gendrel, A.V., Pang, Z., Sparrow, D.B., Whitelaw, N., Craig, J.M., Apedaile, A., Hilton, D.J., Dunwoodie, S.L., Brockdorff, N., et al. (2008). SmcHD1, containing a structural-maintenance-of-chromosomes hinge domain, has a critical role in X inactivation. Nat. Genet. *40*, 663–669.

Bouillet, P., Metcalf, D., Huang, D.C.S., Tarlinton, D.M., Kay, T.W.H., Köntgen, F., Adams, J.M., and Strasser, A. (1999). Proapoptotic Bcl-2 relative Bim required for certain apoptotic responses, leukocyte homeostasis, and to preclude autoimmunity. Science *286*, 1735–1738.

Cecconi, F., Alvarez-Bolado, G., Meyer, B.I., Roth, K.A., and Gruss, P. (1998). Apaf1 (CED-4 homolog) regulates programmed cell death in mammalian development. Cell *94*, 727–737.

Chen, X., Watkins, R., Delot, E., Reliene, R., Schiestl, R.H., Burgoyne, P.S., and Arnold, A.P. (2008). Sex difference in neural tube defects in p53-null mice is caused by differences in the complement of X not Y genes. Dev. Neurobiol. *68*, 265–273.

Chureau, C., Chantalat, S., Romito, A., Galvani, A., Duret, L., Avner, P., and Rougeulle, C. (2011). Ftx is a non-coding RNA which affects Xist expression and chromatin structure within the X-inactivation center region. Hum. Mol. Genet. *20*, 705–718.

Clemson, C.M., McNeil, J.A., Willard, H.F., and Lawrence, J.B. (1996). XIST RNA paints the inactive X chromosome at interphase: evidence for a novel RNA involved in nuclear/chromosome structure. J. Cell Biol. *132*, 259–275.

Copp, A.J., Stanier, P., and Greene, N.D. (2013). Neural tube defects: recent advances, unsolved questions, and controversies. Lancet Neurol. *12*, 799–810.

Cotton, A.M., Ge, B., Light, N., Adoue, V., Pastinen, T., and Brown, C.J. (2013). Analysis of expressed SNPs identifies variable extents of expression from the human inactive X chromosome. Genome Biol. *14*, R122.

Csankovszki, G., Panning, B., Bates, B., Pehrson, J.R., and Jaenisch, R. (1999). Conditional deletion of Xist disrupts histone macroH2A localization but not maintenance of X inactivation. Nat. Genet. *22*, 323–324.

Czabotar, P.E., Lessene, G., Strasser, A., and Adams, J.M. (2014). Control of apoptosis by the BCL-2 protein family: implications for physiology and therapy. Nat. Rev. Mol. Cell Biol. *15*, 49–63.

Delbridge, A.R., Pang, S.H., Vandenberg, C.J., Grabow, S., Aubrey, B.J., Tai, L., Herold, M.J., and Strasser, A. (2016). RAG-induced DNA lesions activate proapoptotic BIM to suppress lymphomagenesis in p53-deficient mice. J. Exp. Med. *213*, 2039–2048.

Dixon-McDougall, T., and Brown, C. (2016). The making of a Barr body: the mosaic of factors that eXIST on the mammalian inactive X chromosome. Biochem. Cell Biol. *94*, 56–70.

Furlan, G., Gutierrez Hernandez, N., Huret, C., Galupa, R., van Bemmel, J.G., Romito, A., Heard, E., Morey, C., and Rougeulle, C. (2018). The Ftx noncoding locus controls X chromosome inactivation independently of its RNA products. Mol. Cell *70*, 462–472.e8.

Grabow, S., Delbridge, A.R., Valente, L.J., and Strasser, A. (2014). MCL-1 but not BCL-XL is critical for the development and sustained expansion of thymic lymphoma in p53-deficient mice. Blood *124*, 3939–3946.

Greene, N.D., and Copp, A.J. (2014). Neural tube defects. Annu. Rev. Neurosci. *37*, 221–242.

Hakem, R., Hakem, A., Duncan, G.S., Henderson, J.T., Woo, M., Soengas, M.S., Elia, A., de la Pompa, J.L., Kagi, D., Khoo, W., et al. (1998). Differential requirement for caspase 9 in apoptotic pathways in vivo. Cell *94*, 339–352.

Hall, J.G. (1986). Neural tube defects, sex ratios, and X inactivation. Lancet *2*, 1334–1335.

Harris, M.J., and Juriloff, D.M. (2010). An update to the list of mouse mutants with neural tube closure defects and advances toward a complete genetic perspective of neural tube closure. Birth Defects Res. A Clin. Mol. Teratol. *88*, 653–669.

Haupt, S., di Agostino, S., Mizrahi, I., Alsheich-Bartok, O., Voorhoeve, M., Damalas, A., Blandino, G., and Haupt, Y. (2009). Promyelocytic leukemia protein is required for gain of function by mutant p53. Cancer Res. *69*, 4818–4826.

Hoki, Y., Kimura, N., Kanbayashi, M., Amakawa, Y., Ohhata, T., Sasaki, H., and Sado, T. (2009). A proximal conserved repeat in the Xist gene is essential as a genomic element for X-inactivation in mouse. Development *136*, 139–146.

Jacks, T., Remington, L., Williams, B.O., Schmitt, E.M., Halachmi, S., Bronson, R.T., and Weinberg, R.A. (1994). Tumor spectrum analysis in *p53*-mutant mice. Curr. Biol. *4*, 1–7.

Jansz, N., Nesterova, T., Keniry, A., Iminitoff, M., Hickey, P.F., Pintacuda, G., Masui, O., Kobelke, S., Geoghegan, N., Breslin, K.A., et al. (2018). Smchd1 targeting to the inactive X is dependent on the Xist-HnrnpK-PRC1 pathway. Cell Rep. *25*, 1912–1923.E9.

Jost, P.J., Grabow, S., Gray, D., McKenzie, M.D., Nachbur, U., Huang, D.C., Bouillet, P., Thomas, H.E., Borner, C., Silke, J., et al. (2009). XIAP discriminates between type I and type II FAS-induced apoptosis. Nature *460*, 1035–1039.

Juriloff, D.M., and Harris, M.J. (2012). Hypothesis: the female excess in cranial neural tube defects reflects an epigenetic drag of the inactivating X chromosome on the molecular mechanisms of neural fold elevation. Birth Defects Res. A Clin. Mol. Teratol. *94*, 849–855.

Kay, G.F., Penny, G.D., Patel, D., Ashworth, A., Brockdorff, N., and Rastan, S. (1993). Expression of Xist during mouse development suggests a role in the initiation of X chromosome inactivation. Cell *72*, 171–182.

Ke, F., Voss, A., Kerr, J.B., O'Reilly, L.A., Tai, L., Echeverry, N., Bouillet, P., Strasser, A., and Kaufmann, T. (2012). BCL-2 family member BOK is widely expressed but its loss has only minimal impact in mice. Cell Death Differ. *19*, 915–925.

Ke, F.F.S., Vanyai, H.K., Cowan, A.D., Delbridge, A.R.D., Whitehead, L., Grabow, S., Czabotar, P.E., Voss, A.K., and Strasser, A. (2018). Embryogenesis and adult life in the absence of intrinsic apoptosis effectors BAX, BAK, and BOK. Cell *173*, 1217–1230.e17.

Keniry, A., Gearing, L.J., Jansz, N., Liu, J., Holik, A.Z., Hickey, P.F., Kinkel, S.A., Moore, D.L., Breslin, K., Chen, K., et al. (2016). Setdb1-mediated H3K9 methylation is enriched on the inactive X and plays a role in its epigenetic silencing. Epigenetics Chromatin *9*, 16.

Knudson, C.M., Tung, K.S.K., Tourtellotte, W.G., Brown, G.A.J., and Korsmeyer, S.J. (1995). Bax-deficient mice with lymphoid hyperplasia and male germ cell death. Science *270*, 96–99.

Kuida, K., Haydar, T.F., Kuan, C.Y., Gu, Y., Taya, C., Karasuyama, H., Su, M.S., Rakic, P., and Flavell, R.A. (1998). Reduced apoptosis and cytochrome c-mediated caspase activation in mice lacking caspase 9. Cell *94*, 325–337.

Labi, V., Erlacher, M., Kiessling, S., Manzl, C., Frenzel, A., O'Reilly, L., Strasser, A., and Villunger, A. (2008). Loss of the BH3-only protein Bmf impairs B cell homeostasis and accelerates gamma irradiation-induced thymic lymphoma development. J. Exp. Med. *205*, 641–655.

Lakhani, S.A., Masud, A., Kuida, K., Porter, G.A., Jr., Booth, C.J., Mehal, W.Z., Inayat, I., and Flavell, R.A. (2006). Caspases 3 and 7: key mediators of mitochondrial events of apoptosis. Science *311*, 847–851.

Law, C.W., Chen, Y., Shi, W., and Smyth, G.K. (2014). voom: precision weights unlock linear model analysis tools for RNA-seq read counts. Genome Biol. *15*, R29.

Lee, J.T., Davidow, L.S., and Warshawsky, D. (1999). Tsix, a gene antisense to Xist at the X-inactivation centre. Nat. Genet. *21*, 400–404.

Li, M., He, Y., Dubois, W., Wu, X., Shi, J., and Huang, J. (2012). Distinct regulatory mechanisms and functions for p53-activated and p53-repressed DNA damage response genes in embryonic stem cells. Mol. Cell *46*, 30–42.

Liao, Y., Smyth, G.K., and Shi, W. (2013). The Subread aligner: fast, accurate and scalable read mapping by seed-and-vote. Nucleic Acids Res. *41*, e108.

Liao, Y., Smyth, G.K., and Shi, W. (2014). featureCounts: an efficient general purpose program for assigning sequence reads to genomic features. Bioinformatics *30*, 923–930.

Lin, T., Chao, C., Saito, S., Mazur, S.J., Murphy, M.E., Appella, E., and Xu, Y. (2005). p53 induces differentiation of mouse embryonic stem cells by suppressing Nanog expression. Nat. Cell Biol. *7*, 165–171.

Lindsten, T., Ross, A.J., King, A., Zong, W.X., Rathmell, J.C., Shiels, H.A., Ulrich, E., Waymire, K.G., Mahar, P., Frauwirth, K., et al. (2000). The combined functions of proapoptotic Bcl-2 family members bak and bax are essential for normal development of multiple tissues. Mol. Cell *6*, 1389–1399.

Massa, V., Savery, D., Ybot-Gonzalez, P., Ferraro, E., Rongvaux, A., Cecconi, F., Flavell, R., Greene, N.D., and Copp, A.J. (2009). Apoptosis is not required for mammalian neural tube closure. Proc. Natl. Acad. Sci. USA *106*, 8233–8238.

Mitchell, L.E. (2005). Epidemiology of neural tube defects. Am. J. Med. Genet. C. Semin. Med. Genet. *135C*, 88–94.

Monkhorst, K., Jonkers, I., Rentmeester, E., Grosveld, F., and Gribnau, J. (2008). X inactivation counting and choice is a stochastic process: evidence for involvement of an X-linked activator. Cell *132*, 410–421.

Mould, A.W., Pang, Z., Pakusch, M., Tonks, I.D., Stark, M., Carrie, D., Mukhopadhyay, P., Seidel, A., Ellis, J.J., Deakin, J., et al. (2013). Smchd1 regulates a subset of autosomal genes subject to monoallelic expression in addition to being critical for X inactivation. Epigenetics Chromatin *6*, 19.

Navarro, P., Chambers, I., Karwacki-Neisius, V., Chureau, C., Morey, C., Rougeulle, C., and Avner, P. (2008). Molecular coupling of Xist regulation and pluripotency. Science *321*, 1693–1695.

O'Connor, L., Strasser, A., O'Reilly, L.A., Hausmann, G., Adams, J.M., Cory, S., and Huang, D.C.S. (1998). Bim: a novel member of the Bcl-2 family that promotes apoptosis. EMBO J. *17*, 384–395.

Oda, E., Ohki, R., Murasawa, H., Nemoto, J., Shibue, T., Yamashita, T., Tokino, T., Taniguchi, T., and Tanaka, N. (2000). Noxa, a BH3-only member of the Bcl-2 family and candidate mediator of p53-induced apoptosis. Science *288*, 1053–1058.

Okamoto, K., and Beach, D. (1994). Cyclin G is a transcriptional target of the p53 tumor suppressor protein. EMBO J. *13*, 4816–4822.

Pintacuda, G., Wei, G., Roustan, C., Kirmizitas, B.A., Solcan, N., Cerase, A., Castello, A., Mohammed, S., Moindrot, B., Nesterova, T.B., and Brockdorff, N. (2017). hnRNPK recruits PCGF3/5-PRC1 to the Xist RNA B-repeat to establish polycomb-mediated chromosomal silencing. Mol. Cell *68*, 955–969.e10.

Plath, K., Fang, J., Mlynarczyk-Evans, S.K., Cao, R., Worringer, K.A., Wang, H., de la Cruz, C.C., Otte, A.P., Panning, B., and Zhang, Y. (2003). Role of histone H3 lysine 27 methylation in X inactivation. Science *300*, 131–135.

Puthalakath, H., Villunger, A., O'Reilly, L.A., Beaumont, J.G., Coultas, L., Cheney, R.E., Huang, D.C.S., and Strasser, A. (2001). Bmf: a proapoptotic BH3-only protein regulated by interaction with the myosin V actin motor complex, activated by anoikis. Science *293*, 1829–1832.

Puthalakath, H., O'Reilly, L.A., Gunn, P., Lee, L., Kelly, P.N., Huntington, N.D., Hughes, P.D., Michalak, E.M., McKimm-Breschkin, J., Motoyama, N., et al. (2007). ER stress triggers apoptosis by activating BH3-only protein Bim. Cell *129*, 1337–1349.

Ritchie, M.E., Phipson, B., Wu, D., Hu, Y., Law, C.W., Shi, W., and Smyth, G.K. (2015). limma powers differential expression analyses for RNA-sequencing and microarray studies. Nucleic Acids Res. *43*, e47.

Robinson, M.D., and Oshlack, A. (2010). A scaling normalization method for differential expression analysis of RNA-seq data. Genome Biol. *11*, R25.

Sah, V.P., Attardi, L.D., Mulligan, G.J., Williams, B.O., Bronson, R.T., and Jacks, T. (1995). A subset of p53-deficient embryos exhibit exencephaly. Nat. Genet. *10*, 175–180.

Sandelin, A., Wasserman, W.W., and Lenhard, B. (2004). ConSite: web-based prediction of regulatory elements using cross-species comparison. Nucleic Acids Res. *32*, W249–W252.

Senner, C.E., Nesterova, T.B., Norton, S., Dewchand, H., Godwin, J., Mak, W., and Brockdorff, N. (2011). Disruption of a conserved region of Xist exon 1 impairs Xist RNA localisation and X-linked gene silencing during random and imprinted X chromosome inactivation. Development *138*, 1541–1550.

Silva, J., Mak, W., Zvetkova, I., Appanah, R., Nesterova, T.B., Webster, Z., Peters, A.H., Jenuwein, T., Otte, A.P., and Brockdorff, N. (2003). Establishment of histone h3 methylation on the inactive X chromosome requires transient recruitment of Eed-Enx1 polycomb group complexes. Dev. Cell *4*, 481–495.

Slatter, T.L., Hung, N., Campbell, H., Rubio, C., Mehta, R., Renshaw, P., Williams, G., Wilson, M., Engelmann, A., Jeffs, A., et al. (2011). Hyperproliferation, cancer, and inflammation in mice expressing a Δ133p53-like isoform. Blood *117*, 5166–5177.

Tian, D., Sun, S., and Lee, J.T. (2010). The long noncoding RNA, Jpx, is a molecular switch for X chromosome inactivation. Cell *143*, 390–403.

Villunger, A., Michalak, E.M., Coultas, L., Müllauer, F., Böck, G., Ausserlechner, M.J., Adams, J.M., and Strasser, A. (2003). p53- and drug-induced apoptotic responses mediated by BH3-only proteins puma and noxa. Science *302*, 1036–1038.

Voss, A.K., Thomas, T., and Gruss, P. (1997). Germ line chimeras from female ES cells. Exp. Cell Res. *230*, 45–49.

Wu, D., Lim, E., Vaillant, F., Asselin-Labat, M.-L., Visvader, J.E., and Smyth, G.K. (2010). ROAST: rotation gene set tests for complex microarray experiments. Bioinformatics *26*, 2176–2182.

Wutz, A., and Jaenisch, R. (2000). A shift from reversible to irreversible X inactivation is triggered during ES cell differentiation. Mol. Cell *5*, 695–705.

Yamaguchi, Y., Shinotsuka, N., Nonomura, K., Takemoto, K., Kuida, K., Yosida, H., and Miura, M. (2011). Live imaging of apoptosis in a novel transgenic mouse highlights its role in neural tube closure. J. Cell Biol. *195*, 1047–1060.

Ying, Q.L., Wray, J., Nichols, J., Batlle-Morera, L., Doble, B., Woodgett, J., Cohen, P., and Smith, A. (2008). The ground state of embryonic stem cell self-renewal. Nature *453*, 519–523.

Yoshida, H., Kong, Y.-Y., Yoshida, R., Elia, A.J., Hakem, A., Hakem, R., Penninger, J.M., and Mak, T.W. (1998). Apaf1 is required for mitochondrial pathways of apoptosis and brain development. Cell *94*, 739–750.

Zhang, Y., Liu, T., Meyer, C.A., Eeckhoute, J., Johnson, D.S., Bernstein, B.E., Nusbaum, C., Myers, R.M., Brown, M., Li, W., and Liu, X.S. (2008). Model-based analysis of ChIP-seq (MACS). Genome Biol. *9*, R137.

Zuckerman, V., Lenos, K., Popowicz, G.M., Silberman, I., Grossman, T., Marine, J.C., Holak, T.A., Jochemsen, A.G., and Haupt, Y. (2009). c-Abl phosphorylates Hdmx and regulates its interaction with p53. J. Biol. Chem. *284*, 4031–4039.

STAR★METHODS

KEY RESOURCES TABLE

REAGENT or RESOURCE	SOURCE	IDENTIFIER
Antibodies		
anti-H3K27me3	Millipore	07-449 (RRID:AB_310624)
anti-rabbit IgG-Alexa 488	Invitrogen	A-21206 (RRID:AB_2535792)
anti-p53 antibody	Novocastra	NCL-L-p53-CM5p
Chemicals, Peptides, and Recombinant Proteins		
SpectrumRed dUTP	Abbott	Vysis
SEEBRIGHT Red 650 dUTP 25 nmol	Enzo	ENZ-42522
SEEBRIGHT Orange 552 dUTP (lyophilized) 50 nmol	Enzo	ENZ-42842L-0050
SEEBRIGHT Green 496 dUTP (lyophilized) 50 nmol	Enzo	ENZ-42831L-0050
TRIzol reagent	Invitrogen	15596026
FuGENE® HD Transfection reagent	Promega	E2311
Critical Commercial Assays		
In Situ Cell Death Detection Kit	Roche	12156792910
Nick Translation Kit	Abbott	07J00-001
RNeasy micro kit	QIAGEN	74004
SuperScript III First-Strand Synthesis SuperMix Kit	Invitrogen	18080400
Dual luciferase (LUC) assay	Promega	E1910
Deposited Data		
RNA-seq data	This study	GEO: GSE127446
anti-p53 ChIP-seq dataset	(Li et al., 2012)	GEO: GSE26360
Experimental Models: Cell Lines		
p53$^{+/+}$ embryonic stem cells	This study	N/A
p53$^{-/-}$ embryonic stem cells	This study	N/A
H1299 cells	American Type Culture Collection	CRL-5803
Experimental Models: Organisms/Strains		
p53$^{+/-}$ mice	(Jacks et al., 1994)	N/A
Bim$^{+/-}$ mice	(Bouillet et al., 1999)	N/A
Bmf$^{+/-}$ mice	(Labi et al., 2008)	N/A
Xiap$^{+/-}$ mice	(Jost et al., 2009)	N/A
Bax$^{+/-}$ mice	(Knudson et al., 1995)	N/A
Bak$^{+/-}$ mice	(Lindsten et al., 2000)	N/A
Bok$^{+/-}$ mice	(Ke et al., 2012)	N/A
Bax$^{+/-}$*Bak*$^{-/-}$*Bok*$^{-/-}$ mice	(Ke et al., 2018)	N/A
Smchd1$^{+/MommeD1}$ mice	(Blewitt et al., 2008)	N/A
Oligonucleotides		
See Table S4 for oligonucleotide sequences for ChIP-qPCR, RT-qPCR and genotyping		N/A
Recombinant DNA		
pCMV-Xist-PA	(Wutz and Jaenisch, 2000)	N/A
Huwe1 BAC	Children's Hospital Oakland Research Institute https://bacpacresources.org	RP24-157H12
Usp9x BAC	Children's Hospital Oakland Research Institute https://bacpacresources.org	RP23-216M21
Jpx2x	This study	N/A
Jpx3x	This study	N/A

(*Continued on next page*)

Continued		
REAGENT or RESOURCE	SOURCE	IDENTIFIER
Ftx_1	This study	N/A
Ftx-2	This study	N/A
pGL4.24 Luciferase Reporter Vector	Promega	E8421
p53 expression construct	(Zuckerman et al., 2009)	N/A
p63 expression construct	A. Constanzo	N/A
p73 expression construct	G. Blandino	N/A
Ccng1	M. Oren	N/A
Tk	G. Blandino	N/A
Renilla luciferase SV40 Reporter Vector	Promega	E2231
Software and Algorithms		
GraphPad Prism 7	GraphPad Software	RRID:SCR_002798
FlowJo version 10	FlowJo LLC	RRID:SCR_008520
Stata 12.1 software	StataCorp, Texas	RRID:SCR_012763
ImageJ 1.47n	NIH	https://imagej.nih.gov/ij/
R	R Project for Statistical Computing	RRID:SCR_001905
R packages Rsubread, edgeR and limma	Bioconductor	RRID:SCR_001905
SeqMonk	Babraham Institute	RRID:SCR_001913

CONTACT FOR REAGENT AND RESOURCE SHARING

Further information and requests for resources and reagents should be directed to and will be fulfilled by the Lead Contact, Anne K. Voss: avoss@wehi.edu.au.

EXPERIMENTAL MODEL AND SUBJECT DETAILS

Mice

Experiments with mice were conducted with approval from the Walter and Eliza Hall Institute for Medical Research Animal Ethics Committee. $p53^{-/-}$ (Jacks et al., 1994) and $Bim^{-/-}$ (Bouillet et al., 1999) mice have been previously described. Both strains were originally generated on a mixed C57BL/6x129SV genetic background using 129SV-derived ES cells, but had been backcrossed to C57BL/6 mice for more than 25 generations prior to the current study. The $Bmf^{-/-}$ (Labi et al., 2008) and $Xiap^{-/-}$ (Jost et al., 2009) mice were generated on a C57BL/6 background using C57BL/6-derived ES cells. Compound mutant mice were generated by inter-crossing single mutant strains. Breeding strategies are detailed in Table S1. $Bax^{-/-}Bak^{-/-}Bok^{-/-}$ triple null embryos were generated from $Bax^{+/-}Bak^{-/-}Bok^{-/-}$ intercrosses, as described previously (Ke et al., 2018), originally derived from $Bax^{+/-}$ (Knudson et al., 1995), $Bak^{+/-}$ (Lindsten et al., 2000) and $Bok^{+/-}$ mice (Ke et al., 2012). $Smchd1^{MD1/MD1}$ embryos were derived from intercrosses of $Smchd1^{+/MommeD1}$ mice (Blewitt et al., 2008). Mice were genotyped by PCR or allelic discrimination assays, as described previously (Blewitt et al., 2008; Grabow et al., 2014; Ke et al., 2012). Genotyping primers are listed in Table S4.

Isolation of p53 mutant and control ES cells

Embryonic stem (ES) cells were isolated from E3.5 embryos derived from $p53^{+/-}$ x $p53^{+/-}$ matings, essentially as described previously (Voss et al., 1997), with the modification that 2i medium (Ying et al., 2008) and no feeder cells were used. ES cells were cultured in 2i medium and genotyped for *p53*.

METHOD DETAILS

Phenotypic analysis

Embryos and pups were isolated at the indicated time points following timed matings. Noon of the morning on which the vaginal mating plug was observed was designated embryonic day 0.5 (E0.5). Abnormalities were identified and scored before genotyping of the mice, i.e., blinded to genotype. Images were taken using AxioCam HR, Carl Zeiss on a Stemi 2000-C dissecting microscope (Carl Zeiss; Germany). E9.5 (3.2x), E19 (0.65x), E12.5 (1.5x).

Whole-mount TUNEL staining and microscopy

Embryos were harvested at E9 and incubated with 10 μg/mL proteinase K (Sigma Aldrich) at RT for 10 min. Fixing was subsequently performed using 4% paraformaldehyde for 20 min at RT, and embryos were then permeabilized by treatment with ethanol:acetic acid (2:1) for 20 min at −20°C. Embryos were rinsed several times with PBS (Sigma Aldrich) before TUNEL staining was performed with the *In Situ* Cell Death Detection Kit (catalog number 12156792910, Roche) according to the manufacturer's instructions. To generate positive controls, embryos were treated with DNase I (5 μg/μL) at 1:1000 dilution with PBS for 30 min at 37°C, prior to incubation with the TUNEL reagent. After extensive washing with PBS with 0.1% Tween, embryos were stained with DAPI for 3 h at RT and cleared overnight in a 5%–80% glycerol gradient. All images were obtained using a 10x objective with the LSM 780 laser scanning confocal microscope (Zeiss).

TUNEL staining for flow cytometric analysis

Embryos were harvested at E9.5 and digested in 0.5 mL of trypsin in PBS at 37°C for 5-7 min with gentle agitation. The reaction was halted by addition of 1 mL DMEM containing 10% FCS, and single cell suspensions were then generated by gentle pipetting. Cells were washed once with PBS, centrifuged at 200*g*, resuspended in 100 μL of ice-cold PBS, and fixed with 2% paraformaldehyde (PFA) for 1 h at room temperature. Cells were subsequently washed with PBS containing 2% FCS and permeabilized with 0.1% Triton-X in 0.1% sodium citrate for 2 min on ice. Following another round of washing, TUNEL staining was performed using the *In Situ* Cell Death Detection Kit (catalog number 12156792910, Roche) according to the manufacturer's instructions. Cells were counter-stained with DAPI prior to flow cytometric analysis using the LSR IIW machine (Becton Dickinson).

Detection of Xist RNA and nascent Huwe1 and Usp9x RNA by fluorescence *in situ* hybridization

E9.5 brain cells were isolated and plated in chamber slides, coated with poly-lysine for 24 h. *Xist* RNA FISH was performed as previously described (Jansz et al., 2018; Keniry et al., 2016). *Xist* RNA was detected with the 15 kb cDNA, *pCMV-Xist-PA*, as described (Wutz and Jaenisch, 2000). The *Xist* probe was labeled with SpectrumRed dUTP (Abbott, Vysis) or SEEBRIGHT Red 650 dUTP (Enzo) by nick translation (Abbott). The cells were mounted in Vectashield HardSet mounting medium with DAPI (Vector Laboratories). Cells were visualized using a 100x oil objective (Zeiss). Images were analyzed using ImageJ 1.47n software. An average of ~100 cells were analyzed per embryo, using a threshold-based method and background subtraction.

Similarly, nascent *Huwe1* and *Usp9x* RNAs were detected using BACS as probes ordered from the Children's Hospital Oakland Research Institute (https://bacpacresources.org; clones RP24-157H12 and RP23-216M21, respectively) labeled with a nick translation kit (Abbott) incorporating SEEBRIGHT Green 496 dUTP (Enzo) and SEEBRIGHT Orange 552 dUTP (Enzo), respectively. Length of the probe and mRNA expression levels affect the ability to detect transcripts by Nascent RNA FISH. *Huwe1* (14,624 bases) and *Usp9x* (11,903) were selected as the next two longest RNAs apart from *Xist* (17,918 bases).

Anti-H3K27m3 immunofluorescence staining

Brain cells from E9.5 embryos were isolated and plated in chamber slides, coated with poly-lysine for 24 h. Cells were washed once in PBS, fixed in 3% PFA (pH 7.0) for 10 min at room temperature and, with intervening PBS wash steps, treated with 0.5% Triton X-100 for 5 min on ice, 1% BSA for 15 min, anti-H3K27me3 antibody (Millipore, 07-449, 1:100) diluted in 1% BSA/PBS for 45 min, anti-rabbit IgG secondary antibody (Invitrogen, Alexa 488, 1:500) diluted in 1% BSA/PBS for 40 min, counter-stained with DAPI, mounted and imaged.

RNA sequencing

E9.5 embryos were matched for somite counts. The brains to just posterior of the otic vesicle were dissected from these embryos (see Figures S1D and S1E) and RNA was isolated using the RNeasy micro kit (QIAGEN 74004; Germany). RNA samples (N = 4 for AF and CM, N = 3 for CF) were sequenced on an Illumina HiSeq 2500 to produce 11-16 million paired-end 100 bp reads per sample.

Quantitative reverse transcription PCR (RT-qPCR)

Total RNA was isolated from E9.5 embryos using TRIzol reagent (Invitrogen, Carlsbad, CA, USA) according to the manufacturer's instructions. Quantity and purity of the RNA samples were assessed using the NanoDrop (Thermo Fisher Scientific, Waltham, MA, USA). 1 μg of RNA was reverse transcribed to cDNA using the SuperScript III First-Strand Synthesis SuperMix Kit (Invitrogen) with random hexamers in a 20 μL reaction volume. qPCR was subsequently carried out in 384-well plates using Taqman primers (Applied Biosystems) specific for *Ftx* (Mm03455831_m1), *Sirt3* (Mm00452131_m1), *Nup62cl* (Mm01302198_m1), *Maob* (Mm00555412_m1), *Pls3* (Mm00521302_m1), *Xist* (Mm01232884_m1), *Tsix* (Mm03455648_m1), *Ring1* (Mm01278940_m1), *Bmi1* (Mm03053308_m1), or *HMBS* (Mm01143545_m1) that were designed to cross an exon junction, hence reducing the likelihood of amplifying genomic DNA. Each well contained a 10 μL reaction, and PCR amplifications were performed using the Viia 7 Real-Time PCR System (Thermo Fisher Scientific) under standard running conditions as suggested by the manufacturer. Three replicates of each reaction were performed, and gene expression was normalized to HMBS, which was assigned as the housekeeping gene.

Reporter assays

A 531 bp (*Jpx2*) or 759 bp (*Jpx3*) bp fragment of the *Jpx* promoter proximal to the TSS was cloned in-frame with the luciferase expression cassette in the *pGL4.14* Luciferase Reporter Vector (Promega, Madison, WI). The region in the *Jpx2x* construct encodes two putative p53 binding sites at −456 to −436 and −120 to −100 relative to the start of *Jpx* Exon 1. The region in the *Jpx3x* construct encodes an additional downstream binding site starting within Exon 1 at +129 to + 149. Site positioning based on Ensembl. A 248 bp (mm9_dna range = chrX:100810118-100810365) or 252 bp fragment (mm9_dna range = chrX:100810118-100810365) underlying two prominent p53 binding peaks near the *Ftx* gene in the ChIP-seq dataset (Li et al., 2012) were cloned in-frame with the luciferase expression cassette into the in the *pGL4.24* Luciferase Reporter Vector (Promega, Madison, WI). The sites are at −20139 to −19888 bp and at + 1928 to + 2175 bp from the dominant TSS of the *Ftx* locus. The two sites are ~130 kb and ~150 kb upstream of the TSS of *Xist*.

The dual luciferase (LUC) assay was performed in triplicate according to the manufacturer's instructions (Promega Corporation, Madison, WI, USA) essentially as previously described (Haupt et al., 2009). Briefly, H1299 cells were transiently co-transfected using PEI with LUC reporter constructs for *Jpx*, plus expression constructs for p53 (Zuckerman et al., 2009), p63 (kind gift of A. Constanzo), p73, (kind gift of G. Blandino) or equal amounts of empty vector and Renilla luciferase SV40 reporter (Promega Corporation, Madison, WI, USA). Similarly, assays were undertaken with reporter constructs for *Ftx*. After ~20 h, the fold change in LUC relative to Renilla (REN) luciferase activity was compared between treatments with and without p53 and also its family members p63 and p73. Negative control for p53 activation TK-luciferase (TK, HSV thymidine kinase, kind gift of G. Blandino) and the positive control cyclin G (*Ccng1;* kind gift of M. Oren) demonstrated assay efficacy. Similarly, male and female MEFs at passage 3, either wild-type or null for p53 were assayed, with the modification that the FuGENE® HD Transfection reagent (Promega Corporation, Madison, WI, USA) replaced PEI.

p53 chromatin immunoprecipitation

$p53^{+/+}$ and $p53^{-/-}$ MEFs were grown to 70%–80% confluence and positive controls were treated with doxorubicin (0.5 μg/mL) for 24 h. $p53^{+/+}$ and $p53^{-/-}$ ES cells were treated with doxorubicin (0.5 μg/mL) for 3 h to 4 h. Cells were washed twice in cold PBS, then cross-linked with 1% PFA for 10 min. Cross-linking was stopped by adding glycine at a final concentration of 125 mM. After washing cells twice with cold PBS, they were harvested by scrapping in PBS supplemented with protease inhibitors and pelleted. Cells were lysed in 1x lysis buffer (1% SDS, 10 mM EDTA, 5 mM Tris-Cl pH 8.1, 1x protease inhibitors) and chromatin was sheared using the Covaris sonicator (S220, Covaris; Woburn, MA), standardized to ~50 μg across all samples as estimated by spectrophotometry absorption at 260 and 280 nm, then topped up with to 2 mL in ChIP dilution buffer (0.01% SDS, 1.1% Triton X-100, 1.2 mM EDTA, 16.7 mM Tris-Cl pH 8.1, 167 mM NaCl and 1x protease inhibitors). Chromatin was pre-cleared with 30 μL of 50% protein A magnetic beads (Merck Millipore; Germany) for 30 min at 4°C, then 5 μL anti-p53 antibody (5 μg; Novocastra CM5; Leica Biosystems, Germany) were added to each tube and incubated overnight at 4°C. Immune complexes were recovered by adding 30 μL protein A magnetic beads for 1 h at 4°C. Then, using a magnetic rack, the following washes were conducted for 5 min each: low salt wash buffer (0.1% SDS, 1% Triton X-100, 2mM EDTA, 20 mM Tris-Cl ph 8.1, 150 mM NaCl), high salt wash buffer (0.1% SDS, 1% Triton X-100, 2mM EDTA, 20 mM Tris-Cl ph 8.1, 500 mM NaCl), LiCl wash buffer (0.25 M LiCl, 1% NP40, 1% Deoxycholic acid, 1 mM EDTA, 10 mM Tris-Cl pH 8.1), followed by 2x washes in TE buffer (10 mM Tris-HCl (pH 8.0), 0.1 mM EDTA). Chromatin was eluted from magnetic beads with elution buffer (1% SDS, 100 mM $NaHCO_3$) for 20 min at 65°C, cross-links were reversed in NaCl at a final concentration of 0.2 M for 4 h, followed by proteinase K and RNase A treatment. DNA was purified by phenol/chloroform extraction and subjected to qPCR with the following primers designed to detect the putative p53 binding sites in the X chromosome inactivation center: *Jpx1* gccctgtgaggtgtccaata, acagaggctaggtggcaaag; *Jpx2* gcagccgggagaggaacc, ctgtcaggctgtccctaaatg; *Jpx3* ggattagccaggcagctaga, ctctctgacagcgcgagac; *Xist1* gcttgccccatatgatgaga, cttggtcacggaaccaactc; *Xist2* gtcacatgacttccgccatc, gcaaagggctttgtgtgtc; *Ftx_1* ggcctagttgtgctcatggt, tcaatggggaaacttccttc*; Ftx_2* gagcctcaggacttcaggtg, ttcaaagtgagctccccagt; the positive control loci: *Noxa* gcaggactcgtcctccttg, agcgaagtggagcaggtct; *Puma* ctctggctgccgggaaac, ggggacaagtcggggctt; and the chromatin repressor loci: *Ring1a_1* tccaaggtaggaagccatgt, gggtttctccctctcactcc; *Ring1a_2,* agccc cattccctatcattt, acaaagccaggaagcttgaa; *Bmi1* aaatgtgtgggggttttcag, aggacctccccagttgaagt; *Sirt3_1* cagaaggtgtgcaggagaca, actgttgctaggcagctggt; *Sirt3_2* gtccctgattcctcactcca, tatatgggggaatgcgctta.

QUANTIFICATION AND STATISTICAL ANALYSIS

The statistical tests used, the definitions of center and dispersion measures are specified in each figure legend. The number of animals used (or number of experiments) is stated either in the figures or in the figure legend. Significance values (FDRs or p values) are stated as exact values in the figures. Animals were assessed blinded to genotype, namely before the genotype was determined. Automation (flow cytometry, RNA-seq) was used to assess parameters where possibly to avoid bias.

Analysis of RNA sequencing data

Reads were aligned to the mm10 genome using Rsubread 1.10.2 (Liao et al., 2013) and reads were counted by Entrez Gene ID using featureCounts (Liao et al., 2014) and Rsubread's built-in RefSeq annotation. Obsolete Entrez IDs were removed, as were mitochondrial genes, predicted (Gm) genes and unexpressed genes. Genes were considered expressed if they achieve at least 1 count-per-million in at least 3 samples. Library sizes were normalized by the TMM method (Robinson and Oshlack, 2010). Differential expression

analysis used the limma package (Ritchie et al., 2015) and the voom method (Law et al., 2014). Pairwise comparisons were made between the AF, CF and CM genotypes using robust empirical Bayes t-statistics. Genes with false discovery rate (FDR) below 5% were considered differentially expressed. Gene set tests were conducted using the ROAST method (Wu et al., 2010) with 9999 rotations. Multidimensional scaling plots and barcode plots were drawn using limma's plotMDS and barcodeplot functions respectively.

Analysis of anti-p53 ChIP-seq data

Anti-p53 ChIP-seq data derived from untreated and doxorubicin treated mouse embryonic stem cells, as well as input tracks were obtained from (Li et al., 2012), GEO database with a SuperSeries number, GSE26360. Mapped reads were examined for genomic enrichment using MACS peak caller (Zhang et al., 2008) in SeqMonk (Babraham Institute) and then compared to our p53 mutant and control RNA-seq data.

Statistical analysis

Column charts, and line graphs were prepared using Excel (Microsoft, CA) or GraphPad Prism 6 (GraphPad Corporation, La Jolla, CA). Statistical comparisons as stated in the figure legends were performed using GraphPad Prism 6, Stata 12.1 software, StataCorp, Texas, or R version 3.4.1.

DATA AND SOFTWARE AVAILABILITY

The accession number for the RNA sequencing data produced in this study is GEO: GSE127446.